1. Cosmic Plasma Fundamentals

1.1 Plasma

Plasma consists of electrically charged particles that respond collectively to electromagnetic forces. The charged particles are usually clouds or beams of electrons or ions, or a mixture of electrons and ions, but also can be charged grains or dust particles. Plasma is also created when a gas is brought to a temperature that is comparable to or higher than that in the interior of stars. At these temperatures, all light atoms are stripped of their electrons, and the gas is reduced to its constituent parts: positively charged bare nuclei and negatively charged free electrons. The name *plasma* is also properly applied to ionized gases at lower temperatures where a considerable fraction of neutral atoms or molecules are present.

While all matter is subject to gravitational forces, the positively charged nuclei, or ions, and the negatively charged electrons of plasmas react strongly to electromagnetic forces, as formulated by Oliver Heaviside (1850–1925),[1] but now called *Maxwell's Equations*, after James Clerk Maxwell (1831–1879),[2]

$$\frac{\partial \mathbf{B}}{\partial t} = -\nabla \times \mathbf{E} \tag{1.1}$$

$$\frac{\partial \mathbf{D}}{\partial t} = \nabla \times \mathbf{H} - \mathbf{j} \tag{1.2}$$

$$\nabla \cdot \mathbf{D} = \rho \tag{1.3}$$

$$\nabla \cdot \mathbf{B} = 0 \tag{1.4}$$

and the equation of motion due to Hendrik Antoon Lorentz (1853–1928),

$$\frac{d}{dt}(m\mathbf{v}) = q(\mathbf{E} + \mathbf{v} \times \mathbf{B}); \quad \frac{d\mathbf{r}}{dt} = \mathbf{v}; \tag{1.5}$$

The quantities $\mathbf{D} = e\mathbf{E}$ and $\mathbf{B} = m\mathbf{H}$ are the constitutive relations between the electric field $\mathbf{E}$ and the displacement $\mathbf{D}$ and the magnetic induction $\mathbf{B}$ and magnetic intensity $\mathbf{H}$, m and e are the permeability and permittivity of the medium, respectively, and r and $\mathbf{j}$ are the charge and current

densities, respectively.[3] The mass and charge of the particle obeying the force law (1.5) are m and q, respectively.

Because of their strong interaction with electromagnetism, plasmas display a complexity in structure and motion that far exceeds that found in matter in the gaseous, liquid, or solid states. For this reason, plasmas, especially their electrodynamic properties, are far from understood. Irving Langmuir (1881–1957), the electrical engineer and Nobel chemist, coined the term *plasma* in 1923, probably borrowing the term from medical science to describe the collective motions that gave an almost lifelike behavior to the ion and electron regions with which he experimented. Langmuir was also the first to note the separation of plasma into cell-like regions separated by charged particle sheathes. Today, this cellular structure is observed wherever plasmas with different densities, temperatures, or magnetic field strengths come in contact.

Plasmas need not be neutral (i.e., balanced in number densities of electrons and ions). Indeed, the study of pure electron plasmas and even *positron* plasmas, as well as the electric fields that form when electrons and ions separate, are among the most interesting topics in plasma research today.

In addition to cellular morphology, plasmas often display a filamentary structure. This structure derives from the fact that plasma, because of its free electrons, is a good conductor of electricity, far exceeding the conducting properties of metals such as copper or gold. Wherever charged particles flow in a neutralizing medium, such as free electrons in a background of ions, the charged particle flow or current produces a ring of magnetic field around the current, pinching the current into filamentary strands of conducting currents.

Matter in the plasma state can range in temperature from hundreds of thousands of electronvolts (1 eV = 11,605 degrees absolute) to just one-hundredth of an electronvolt. In density, plasmas may be tenuous, with just a few electrons present in a million cubic centimeters, or they may be dense, with more than 10^{20} electrons packed per cubic centimeter (Figure 1.1).

Nearly all the matter in the universe exists in the plasma state, occurring predominantly in this form in the Sun and stars and in interstellar space. Auroras, lightning, and welding arcs are also plasmas. Plasmas exist in neon and fluorescent tubes, in the sea of electrons that moves freely within energy bands in the crystalline structure of metallic solids, and in many other objects.

Plasmas are prodigious producers of electromagnetic radiation.

1.2 The Physical Sizes and Characteristics of Plasmas in the Universe

1.2.1 Plasmas on Earth

On the earth, plasmas are found with dimensions of microns to meters, that is, sizes spanning six orders of magnitude. The magnetic fields associated with these plasmas range from about 0.5 gauss (the earth's ambient field) to megagauss field strengths. Plasma lifetimes on earth span 12 to 19 orders of magnitude: Laser produced plasmas have properties measurable in picoseconds, pulsed power plasmas have nanosecond to microsecond lifetimes (Figure 1.2), and magnetically confined fusion oriented plasmas persist for appreciable fractions of a second. Quiescent plasma sources, including fluorescent light sources, continuously produce plasmas whose lifetimes may be measured in hours, weeks, or years, depending on the cleanliness of the ionization system or the integrity of the cathode and anode discharge surfaces.

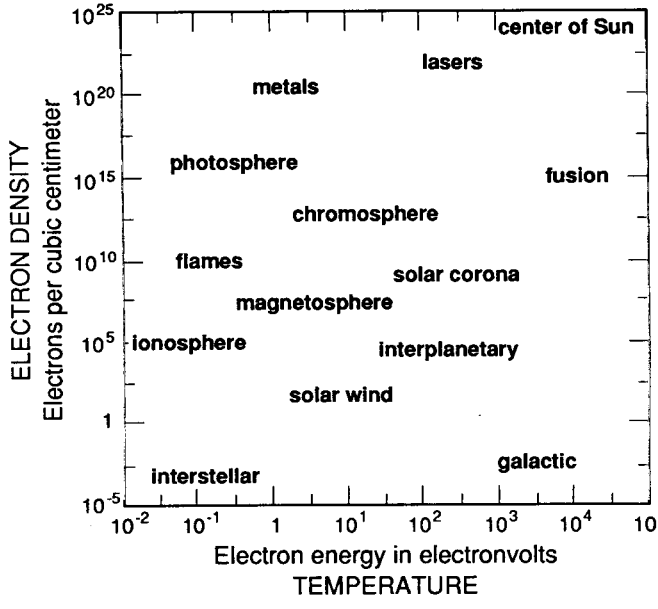

Figure 1.1. The remarkable range of temperatures and densities of plasmas is illustrated by this chart. In comparison, solids, liquids, and gases exist over a very small range of temperatures and pressures. In "solid" metals, the electrons that carry an electric current exist as a plasma within the more rigid crystal structure.

Lightning is a natural plasma resulting from electrical discharges in the earth's lower troposphere (Figure 1.3). Such flashes are usually associated with cumulonimbus clouds but also occur in snow and dust storms, active volcanos, nuclear explosions, and ground fracturing. The maximum time duration of a lightning flash is about 2 s in which peak currents as high as 200 kA can occur. The conversion from air molecules to a singly ionized plasma occurs in a few microseconds, with hundreds of megajoules of energy dissipated and plasma temperatures reaching 3 eV. The discharge channel avalanches at about one-tenth the speed of light, and the high current carrying core expands to a diameter of a few centimeters. The total length of the discharge is typically 2–3 km, although cloud-to-cloud discharges can be appreciably longer. Lightning has been observed on Jupiter, Saturn, Uranus, and Venus [Borucki 1989]. The energy released in a single flash on earth, Venus, and Jupiter is typically 6×10^8 J, 2×10^{10} J, and 2.5×10^{12} J, respectively.

Nuclear driven atmospheric plasmas were a notable exception to the generally short-lived energetic plasmas on earth. For example, the 1.4 megaton (5.9×10^{15} J) Starfish detonation, 400 km above Johnston Island, on July 9, 1962, generated plasma from which artificial *Van Allen belts* of electrons circulating the earth were created. These electrons, bound at about 1.2 earth–radii in a 0.175 G field, produced synchrotron radiation whose decay constant exceeded 100 days (Figure 1.4).

Figure 1.2. Filamentary plasma structure produced by "exploding" titanium wires within a 10 terawatt pulsed-power generator. The photograph was taken with a pin-hole X ray camera.

1.2.2 Near-Earth Plasmas

The earth's *ionosphere* and *magnetosphere* constitute a cosmic plasma system that is readily available for extensive and detailed in situ observation and even active experimentation. Its usefulness as a source of understanding of cosmic plasmas is enhanced by the fact that it contains

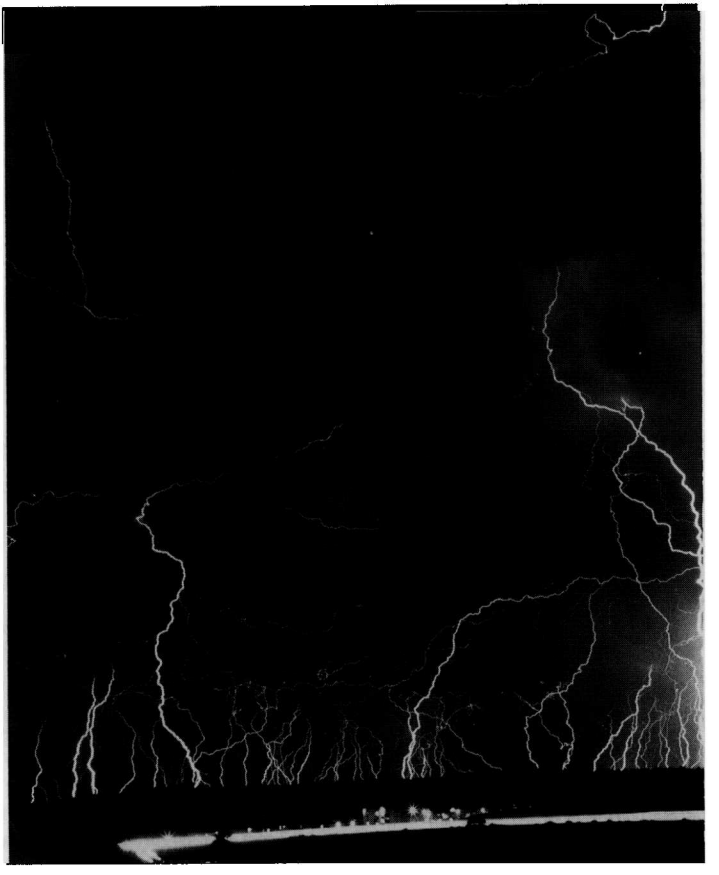

Figure 1.3. Cloud to ground lightning on earth (5 min exposure). The discharge channel may be 20% ionized plasma. The potential difference between the lower portion of the cloud and earth is in excess of 10 MV. The bright line at the lower right is the Santa Fe-Los Alamos highway (courtesy of Henry Ortega, Santa Fe, New Mexico).

a rich variety of plasma populations with densities ranging from more than $10^6 cm^{-3}$ to less than $10^{-2} cm^{-3}$, and temperatures from about 0.1 eV to more than 10 keV.

The earth's magnetosphere is that region of space defined by the interaction of the solar wind with the earth's dipole-like magnetic field. It extends from approximately 100 km above the earth's surface, where the proton neutral atom collision frequency is equal to the proton gyrofrequency, to about ten earth radii (~63,800 km) in the sunward direction and to several hundred earth radii in the anti-sunward direction. It is shown schematically in Figure 1.5.

First detected by radio waves and then by radar, the ionosphere is a layered plasma region closest to the surface of the earth whose properties change continuously during a full day (Figure

Figure 1.4. Starfish event. Artificial aurora produced by plasma particles streaming along the earth's magnetic field lines. Picture taken from a Los Alamos KC-135 aircraft 3 min after the July 9, 1962, 1.4–megaton 400-km-altitude nuclear detonation above Johnston Island. The event produced a degradation of radio communications over large areas of the Pacific and an intense equatorial tube of synchrotron emitting electrons having a decay constant of 100 days. The brightest background object (mark) at the top, left-hand corner is the star Antares, while the right-hand-most object is θ-Centauri. The burst point is two-thirds of the way up the lower plasma striation.

1.6). First to be identified was a layer of molecular ionization, called the E layer. This region extends over a height range of 90–140 km and may have a nominal density of 10^5 cm^{-3} during periods of low solar activity. A D region underlies this with a nominal daytime density of 10^3 cm^{-3}. Overlying the E region is the F layer of ionization, the major layer of the ionosphere, starting at about 140 km. In the height range 100–150 km, strong electric currents are generated by a process analogous to that of a conventional electric generator, or dynamo. The region, in consequence, is often termed the dynamo region and may have densities of 10^6 cm^{-3}. The F layer may extend 1,000 km in altitude where it eventually merges with the plasmas of the magnetopause and solar wind.

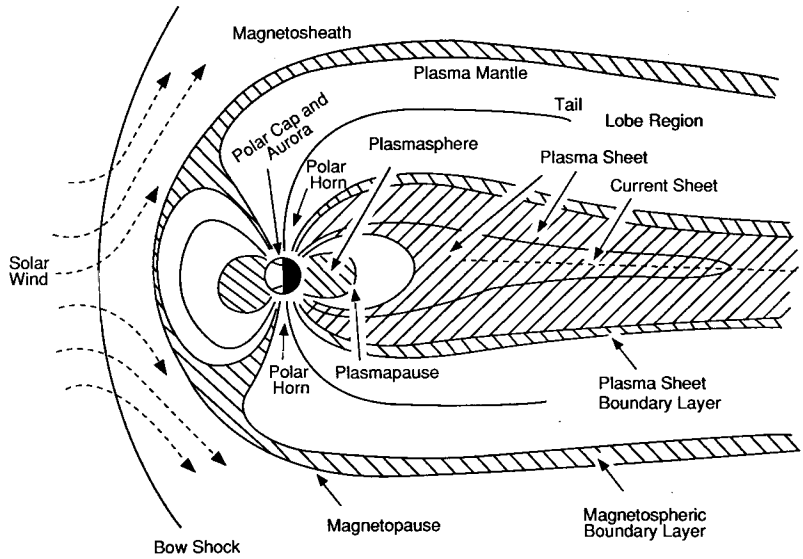

Figure 1.5. Earth's magnetosphere. Ions and electrons in the solar wind (left) impinge against the magnetosphere, distorting the field lines and creating a bow shock and the various regions shown.

The interaction of the supersonic solar wind with the intrinsic dipole magnetic field of the earth forms the magnetosphere whose boundary, called the magnetopause, separates interplanetary and geophysical magnetic fields and plasma environments. Upstream of the magnetopause a collisionless bow shock is formed in the solar wind-magnetosphere interaction process. At the bow shock the solar wind becomes thermalized and subsonic and continues its flow around the magnetosphere as magnetosheath plasma, ultimately rejoining the undisturbed solar wind.

In the anti-solar direction, observations show that the earth's magnetic field is stretched out in an elongated geomagnetic tail to distances of several hundred earth radii. The field lines of the geomagnetic tail intersect the earth at high latitudes (~60°–75°) in both the northern and southern hemisphere (polar horns), near the geomagnetic poles. Topologically, the geomagnetic tail roughly consists of oppositely directed field lines separated by a "neutral" sheet of nearly zero magnetic field. Surrounding the neutral sheet is a plasma of "hot" particles having a temperature of 1–10 keV, density of ~0.01–1 cm^{-3}, and a bulk flow velocity of a few tens to a few hundreds of km s^{-1}.

Deep within the magnetosphere is the plasmasphere, a population of cold (≤1 eV) iono-spheric ions and electrons corotating with the earth. Table 1.1 lists some typical values of parameters in the earth's magnetosphere.

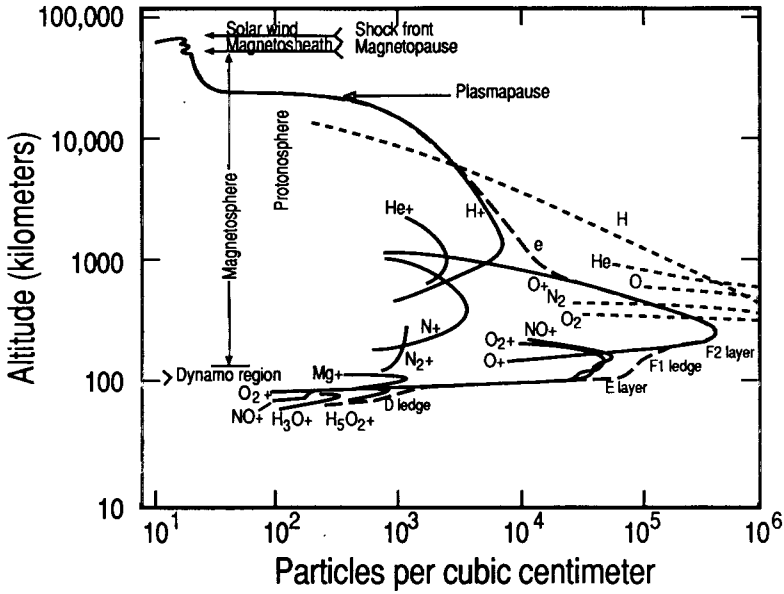

Figure 1.6. Daytime ionosphere at low latitudes and low solar activity.

1.2.3 Plasmas in the Solar System

The space environment around the various planetary satellites and rings in the solar system is filled with plasma such as the solar wind, solar and galactic cosmic rays (high energy charged particles), and particles trapped in the planetary magnetospheres. The first in situ observations of plasma and energetic particle populations in the magnetospheres of Jupiter, Saturn, Uranus, Neptune, and Titan were made by the Voyager 1 and 2 spacecraft from 1979 to 1989. Interplanetary spacecraft have identified magnetospheres around Mercury, Venus, Jupiter, Saturn, Uranus, and Neptune (e.g., Figure 1.7).

Comets also have "magnetospheres" as depicted in Figure 1.8. The cometosheath, a region extending about 1.1×10^6 km (for Comet Halley), consists of decelerated plasma of density $10^2 < n_e < 4{\times}10^3$ and temperature $T_e \sim 1.5$ eV. The peak magnetic field strength found in Comet Halley was 700–800 mG.

Excluding the Sun, the largest organized structures found in the solar system are the plasma tori around Jupiter and Saturn. The Jupiter-Io plasma torus (Figure 1.9) is primarily filled with sulphur ions at a density of 3×10^3 cm^{-3} (Section 4.6.2) An immense weakly ionized hydrogen plasma torus has been found to encircle Saturn, with an outer diameter 25 times the radius of the planet and an inner diameter of about fifteen Saturn radii.

Table 1.1. Typical values of some parameters in the earth's magnetosphere (adapted from A.T.Y. Lui)

		Magnetosheath	Magnetopause	inner side of boundary layer	Plasma mantle	Tail lobe	Plasma-sheet boundary layer	Central plasma sheet	Current sheet
Characteristics									
number density	n (cm^{-3})	5	20	1	1	10^{-2}	0.1	0.5	1
ion temperature	T_i (KeV)	0.1	0.8	4	0.1	0.1	1	5	5
electron temperature	T_e (KeV)	0.05	0.08	0.15	0.05	0.05	0.5	1	1
magnetic field	B (nT)	5	25	40	25	25	20	10	2
electric field	E (mV/m)	1			1	0.1	300	0.01	6
Lengths									
Debye length	λ_D (m)	18	10		40	400	400	280	200
plasma skin depth	λ_E (m)	2.4×10^3			5.3×10^3	5.3×10^4	1.7×10^4	7.5×10^3	5.3×10^3
electron gyroradius	r_{Le} (R_e)	4.9×10^{-4}	1.1×10^{-4}	1.1×10^{-4}	9.8×10^{-5}	9.8×10^{-5}	3.9×10^{-4}	1.1×10^{-3}	5.5×10^{-3}
ion gyroradius	r_{Li} (R_e)	3.0×10^{-2}	2.2×10^{-2}	2.5×10^{-2}	5.9×10^{-3}	5.9×10^{-3}	2.3×10^{-2}	1.0×10^{-1}	5.2×10^{-1}
Frequencies									
electron cyclotron	f_{ce} (Hz)	1.4×10^2	7.0×10^2	6.0×10^2	7.0×10^2	7.0×10^2	5.6×10^2	2.8×10^2	5.6×10^1
ion cyclotron	f_{ci} (Hz)	7.6×10^{-2}	4.0×10^{-1}	6.0×10^{-1}	3.8×10^{-1}	3.8×10^{-1}	3.0×10^{-1}	1.5×10^{-1}	3.0×10^{-2}
electron plasma	f_{pe} (Hz)	2.0×10^4	4.0×10^4	9.0×10^3	9.0×10^3	9.0×10^2	2.8×10^3	6.3×10^3	9.0×10^3
ion plasma	f_{pi} (Hz)	4.7×10^2	1.0×10^3	2.0×10^2	2.1×10^2	2.1×10^1	6.6×10^1	1.5×10^2	2.1×10^2
frequency ratio	ω_{pe}/ω_{ce}	1.4×10^2	5.7×10^1	1.5×10^1	1.3×10^1	1.3×10^0	5.0×10^0	4.5×10^1	1.6×10^2
Velocities									
ion sound	c_s (km/s)	83			83	83	260	370	3.7×10^2
Alfvén	v_A (km/s)	49	122	870	550	5,500	1,400	300	4.4×10^1
electron thermal	v_{the} (km/s)	2,800			2,800	2,800	8,700	1.2×10^4	1.2×10^4
ion thermal	v_{thi} (km/s)	91	277	619	91	91	290	640	6.4×10^2
convection	v_E (km/s)	200	250	50	4	4	5	1	5.0×10^0
Miscellaneous									
thermal/magnetic energy ratio	β_p	6.9	10.0	1.0	0.056	5.6×10^{-4}	0.087	8.8	430
magnetic energy density	($J\ m^{-3}$)	9.9×10^{-18}			2.5×10^{-16}	2.5×10^{-16}	1.6×10^{-16}	4.0×10^{-17}	1.6×10^{-18}

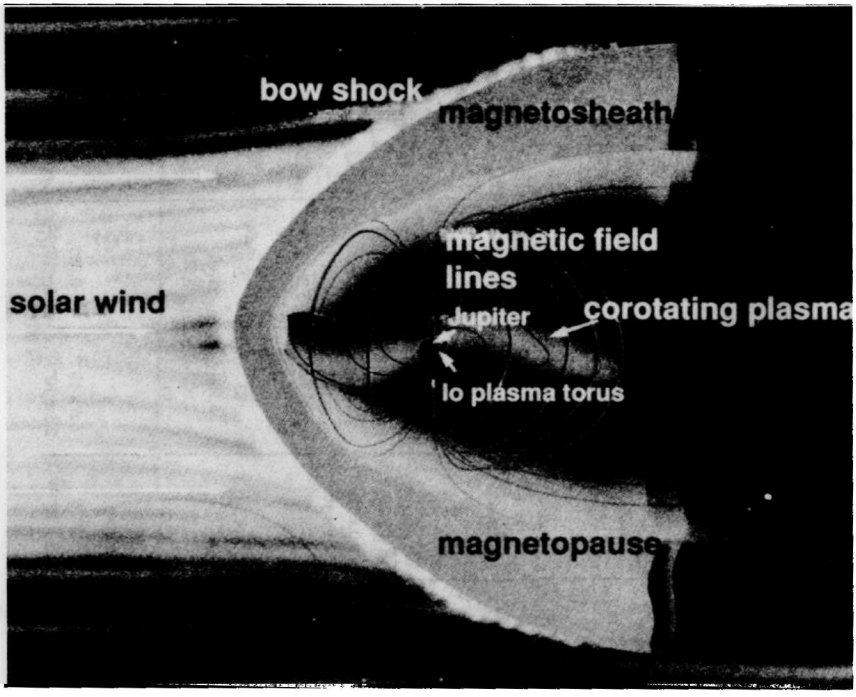

Figure 1.7. Jupiter's magnetosphere. Io's plasma torus contains energetic sulfur and oxygen ions arising from the moon's active discharges.

1.2.4 Transition Regions in the Solar System

Examples of transition regions include the boundary layers found in planetary and comet magnetospheres (Table 1.2). Transition regions between plasmas of different densities, temperatures, magnetization, and chemical composition offer a rich variety of plasma phenomena in the solar system [Eastman 1990].

1.2.5 Solar, Stellar, and Interstellar Plasmas

The nuclear core of the Sun is a plasma at about a temperature of 1.5 keV. Beyond this, our knowledge about the Sun's interior is highly uncertain. Processes which govern the abundance of elements, nuclear reactions, and the generation mechanism and strength of the interior magnetic fields, are incompletely known.

We do have information about the Sun's surface atmospheres that are delineated as follows: the photosphere, the chromosphere, and the inner corona. These plasma layers are superposed on the Sun like onion skins. The photosphere ($T \sim 0.5$ eV) is only a very weakly ionized atmosphere,

Table 1.2. Plasma transition regions within the solar system

Transition region	n (cm^{-3})	T (eV)[a]	v (km/s)	B (μG)[b]
Earth's Magnetosphere				
plasmapause	5 - 1000	1 - 1000	0 - 0.1	500 - 5000
bow shock	10 - 50	5 - 100 (ions) 10 - 40 (e^-)	100 - 500	50 - 300
magnetopause and boundary layer	0.5 - 30	500 - 1600 (ions) 25 - 200 (e^-)	25 - 350	100 - 600
plasma sheet boundary layer	0.02 - 1	300 - 2000 (ions) 30 - 500 (e^-)	0 - 1500	10 - 500
Other Transition Regions				
Jovian boundary layer	0.01 - 1	10 - 30 keV (ions) 50 - 3000 eV (e^-)	100 - 800	1 - 15
cometary boundary layer	10 - 100	1 - 50	20 - 300	50 - 300
heliopause	0.0001 - 1	0.1 - 100	10 -100	0.1 - 20

[a] Temperature associated with 1 eV = 1.602×10^{-19} J = 11,600 °K.
[b] 1 μG = 0.1 nT.

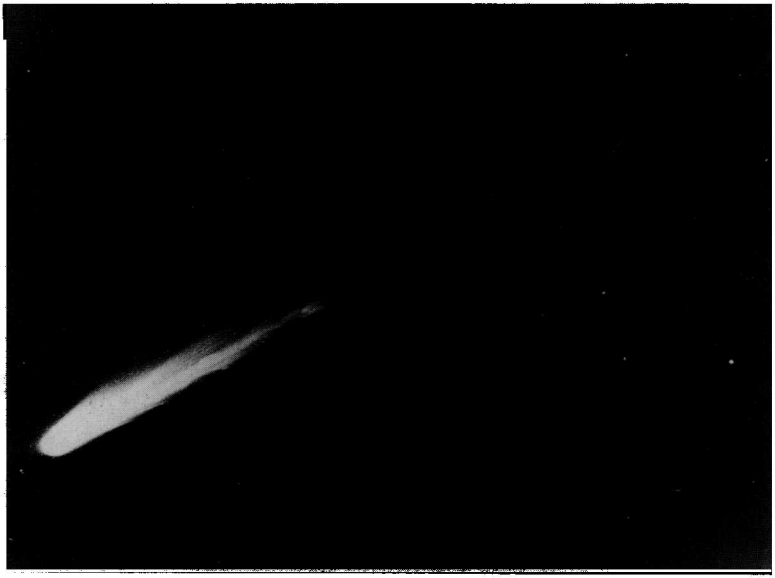

Figure 1.8. Comet Kohoutek (January 1974). The filamentary structure of the tail is typical of the structure of plasmas in space.

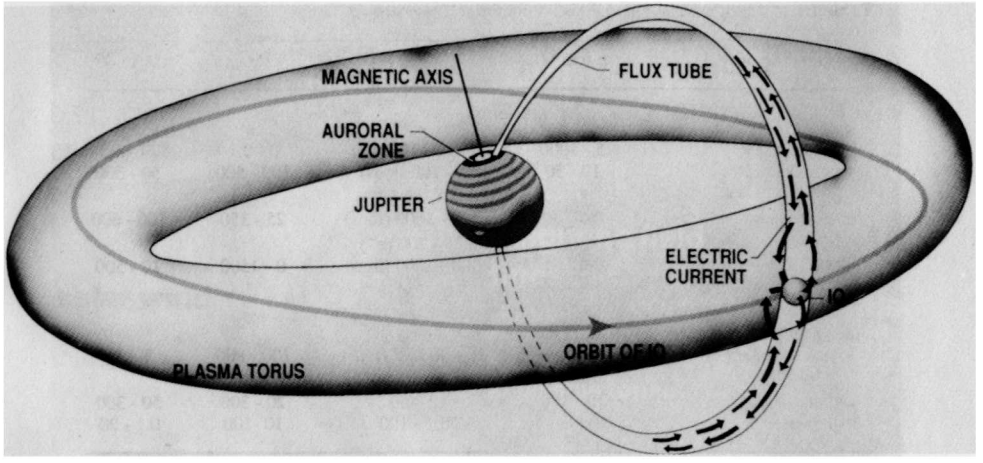

Figure 1.9. The Jupiter-Io plasma torus. The diagram shows the megaampere Birkeland currents flowing between Jupiter and Io.

the degree of ionization being 10^{-4}–10^{-5} in the quiet regions and perhaps 10^{-6}–10^{-7} in the vicinity of sunspots. The chromosphere ($T \sim 4$ eV) extends 5,000 km above the photosphere and is a transition region to the inner corona. The highly ionized inner corona extends some 10^5 km above the photosphere. From a plasma physics point of view, the corona is perhaps the most interesting region of the Sun. The corona is the sight of explosively unstable magnetic-field configurations, X ray emission (Figure 1.10), and plasma temperatures in the range 70–263 eV (Table 1.3).[4] The source of this heating is uncertain.[5]

Table 1.3 Parameters associated with the Sun

Density	
at center	$(10^{26}$ cm$^{-3})$ 160 g/cm^3
at surface	$(10^{15}$ cm$^{-3})10^{-9}$ g/cm^3
in corona	$(10^7$ cm$^{-3})$ 10^{-16} g/cm^3
Temperature	
at center	1.5 keV
at surface	0.5 eV
in sunspots	0.37 eV
in chromosphere	0.38 - 4.5 eV
in corona	70eV - 263 eV
Emission	3.826×10^{26} W
Magnetic Field Strengths	
in sunspots	$\rightarrow$ 3.5 kG
elsewhere on Sun	1 to 100 G

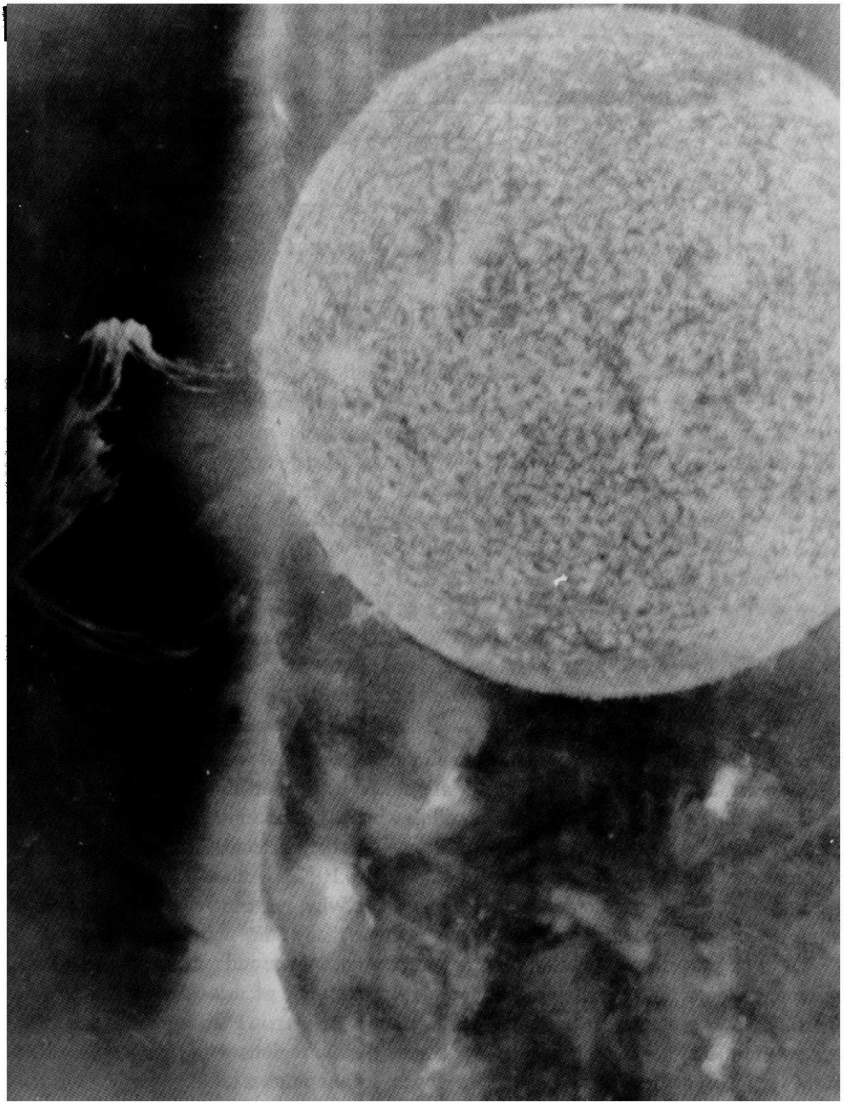

Figure 1.10. Ultraviolet image showing eruption of a solar prominence from the sun (Skylab 1973). The Loop-like structures may be caused by electric currents. The solar "north pole" is to the left..

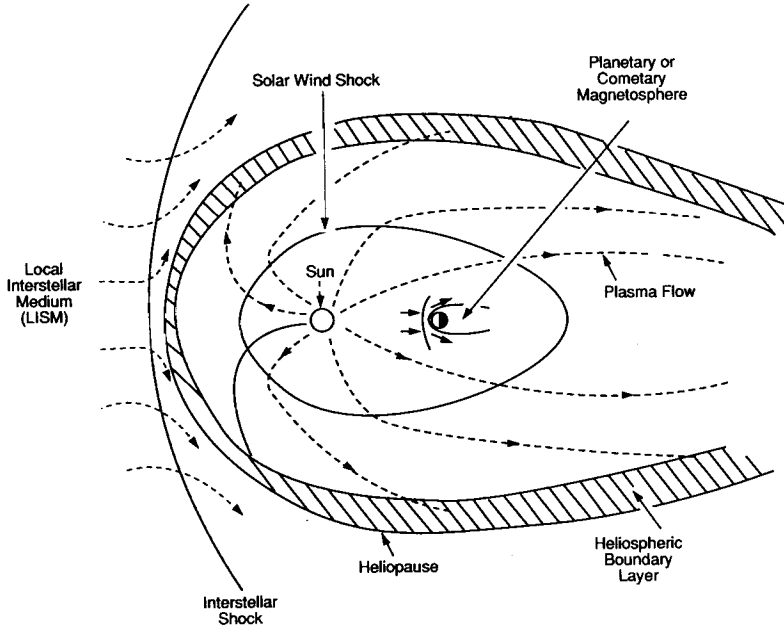

Figure 1.11. The heliosphere.

Solar flares resulting from coronal instabilities raise temperatures to 10–30 keV and produce relativistic streams of electrons and protons. Particles accelerated outward produce radio interference at the earth. Protons accelerated inward collide with ions in the Sun's atmosphere to produce nuclear reactions, whose gamma rays and neutrons have been detected from spacecraft. Solar flares consist of plasma at a temperature of about 1 keV to 10 keV. Although flares represent the most intense energy dissipation of any form of solar activity, releasing energy in the form of gamma rays, X rays, and microwaves, the active sun has many other plasma manifestations.

These include sunspots, photospheric faculae, chromospheric and transition region plages, large coronal loops, and even larger scale coronal streamers and occasional coronal mass ejections. In addition, prominences (referred to as filaments when seen in Hα absorption on the disk) frequently form between opposite magnetic polarities in active regions of the sun. These phenomena are dynamic, on time scales ranging from seconds to the complete solar magnetic cycle of 22 years.

The outer corona and solar wind form the heliosphere (Figure 1.11). At one astronomical unit the solar wind has a plasma density $5 \leq n \leq 60$ cm^{-3} and a velocity of $200 \leq v_{sw} \leq 800$ km s^{-1}. Its temperature can be as high as 50 eV, while B may reach 200 μG. The outer heliosphere has a plasma density $10^{-3} \leq n \leq 10^{-1}$ cm^{-3}, a temperature $0.1 < T < 10$ eV, and a magnetic field strength ~ 1 μG. The local interstellar medium is characterized by $10^{-2} \leq n \leq 1$ cm^{-3}, a tem-

Table 1.4. Solar system plasmas

Parameter	solar wind at 1 AU	outer heliosphere	local interstellar medium	planetary boundary layers
$n_i = n_e$ (cm^{-3})	5 - 60	0.001 - 0.1	0.01 - 1	0.05 - 50
$kT_{i,e}$ (eV)	1 - 50	0.1 - 10	0.1 - 10	5 - 5000
v (km/s)	200 - 800	10 - 100	1 - 30	10 - 1500
B (μG)	10 - 200	<1 - 1	<1 - 20	10 - 500

perature of order 1 eV, and magnetic field strength $1 < B < 20$ μG. Table 1.4 lists some of the parameter values found in the solar system.

The rotating sun, coupled with its continual radial ejection of plasma, twists its magnetic field (that is referred to as the interplanetary magnetic field or IMF) into a classical Archimedean spiral, as depicted in Figure 1.12a. Measurements have confirmed that the interplanetary magnetic field is directed toward the sun in certain regions of the solar system and away from the sun in other regions. These regions are separated by a very sharp boundary layer that is interpreted as a current layer. This layer is depicted in Figure 1.12b which shows "ripples" in the sheet. In this situation, the planets find themselves sometimes in a region where the field has a strong northward component and sometimes where it has a strong southward component.

Stellar plasmas have not only the dimension of the star, 0.3×10^6 km to 10^8 km, but also the stellar magnetospheres, a remnant of the interstellar plasma that the star and its satellites condensed out of. The surface temperatures vary from about 0.3 to 3 eV. Estimates of the magnetic fields range from a few gauss to tens of kilogauss or more for magnetic variable stars.

Stellar winds occur in stars of many types, with wind properties probably connected with stellar magnetism (Table 1.5).

Table 1.5. Parameters associated with the interstellar medium

Parameter	stellar wind	hot ionized medium	warm ionized medium	warm neutral medium	cool neutral medium	filaments, cloud edges, shock interfaces
Neutral density (cm^{-3})	<1	0	<1	10^{-1} - 10^{1}	10^{0} - 10^{4}	10^{1} - 10^{4}
$n_i = n_e$ (cm^{-3})	10^{-1} - 10^{3}	$<10^{-3}$ - 10^{1}	10^{-1} - 10^{1}	10^{-2} - 10^{0}	10^{-2} - 10^{2}	10^{0} - 10^{3}
$kT_{i,e}$ (eV)	10^{0} - 10^{2}	10^{1} - 10^{4}	0.5 - 1	10^{-1} - 10^{0}	10^{-2} - 10^{-1}	10^{0} - $>10^{3}$
v (km/s)	200 - 1000	1 - 20	1 - 20	1 - 20	1 - 100	20 - 1500
B (μG)	5 - 500	<1 - 100	1 - 50	1 - 50	<1 - 20	1 - 1000

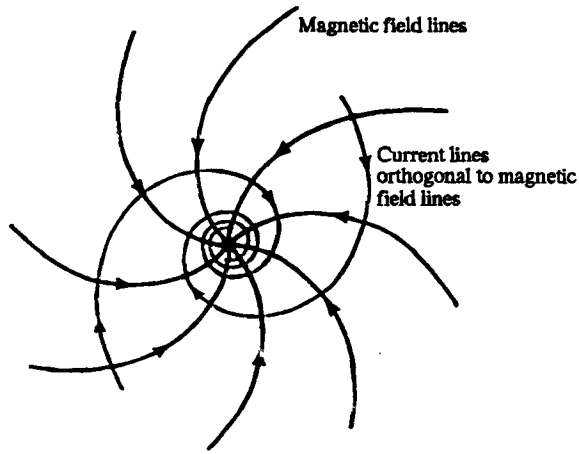

Figure 1.12. (a) Magnetic field lines of the sun which are bent into Archimedean spirals owing to the rotation of the sun and the radial emmision of plasma (which carries the magnetic field). This is a view over the north pole of the sun looking downward at the field lines slightly above the sun's equatorial plane. Close below the equatorial plane, the field lines have the same geometry but opposite direction. The shapes of the associated current lines are also shown. (b) An artist's view of the solar current sheet in the equatorial plane. Alfvén has proposed that the sheet develops ripples like the skirt of a ballerina. As this system rotates, the planets find themselves in different regions so that the interplanetary magnetic field can assume a variety of orientations, e.g., directed toward or away from the sun and northward or southward (courtesy of T. Potemra).

1.2.6 Galactic and Extragalactic Plasmas

Dark clouds within our Galaxy have dimensions of 10^8 km and microgauss strength magnetic fields (Figure 1.13).

The Galactic plasma has an extent equal to the dimensions of our Galaxy itself; ~35 kpc or 10^{21} m. The most salient feature of the Galactic plasma are 10^{-3} G poloidal–toroidal plasma filaments extending nearly 250 light years (60 pc, 1.8×10^{18} m) at the Galactic center (Figure 1.14). The vast regions of nearly neutral hydrogen (HI regions) found in the Galaxy and other galaxies are weakly ionized plasmas. These regions extend across the entire width of the galaxy and are sometimes found between interacting galaxies. They are detected by the 21 cm radiation they emit.

Galaxies may have bulk plasma densities of 10^{-1} cm^{-3}; groups of galaxies, 3×10^{-2} cm^{-3}; and rich clusters of galaxies, 3×10^{-3} cm^{-3}.

By far the single largest plasmas detected in the Universe are those of double radio galaxies. In size, these sources extend hundreds of kiloparsecs (10^{21}–10^{22} m) to a few mega-parsecs (10^{22}–10^{23} m). Double radio galaxies are thought to have densities of 10^{-3} cm^{-3} and magnetic fields of the order of 10^{-4} G (Figure 1.15).

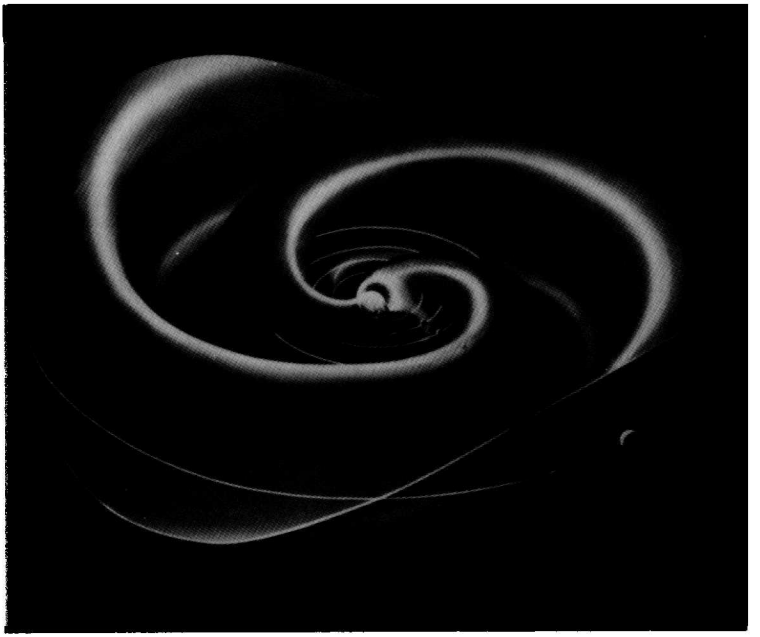

Figure 1.12 (b).

1.3 Regions of Applicability of Plasma Physics

The degree of ionization in interplanetary space and in other cosmic plasmas may vary over a wide range, from fully ionized to degrees of ionization of only a fraction of a percent.[6] Even weakly ionized plasma reacts strongly to electromagnetic fields since the ratio of the electromagnetic force to the gravitational force is 39 orders of magnitude. For example, although the solar photospheric plasma has a degree of ionization as low as 10^{-4}, the major part of the condensable components is still largely ionized. The "neutral" hydrogen (HI) regions around galaxies are also plasmas, although the degree of ionization is only 10^{-4}. Most of our knowledge about electromagnetic waves in plasmas derives from laboratory plasma experiments where the gases used have a low degree of ionization, 10^{-2}–10^{-6}.

Because electromagnetic fields play such an important role in the electrodynamics of plasmas, and because the dynamics of plasmas are often the sources of electromagnetic fields, it is desirable to determine where within the universe a plasma approach is necessary. We first consider the magnetic field. The criterion for neglecting magnetic effects in the treatment of a problem in gas dynamics is that the Lundquist parameter L_u (Section 2.4.2) is much less than unity,

Figure 1.13. The Veil nebula in Cygnus.

Table 1.6. Characteristic quantities for laboratory and cosmic plasmas [adapted from Alfvén and Fälthammar 1963]

	l_c meters	B tesla	ρ_m kg/m^3	σ siemens/m	V_A m/s	L_u
Laboratory experiments						
Mercury	0.1	1	10^4	10^6	7.7	1
Sodium	0.1	1	10^3	10^7	30	37
Hydrogen	0.1	1	10^{-7}	5×10^4	2.8×10^6	2×10^4
Cosmic plasmas						
Earth's interior	10^6	10^{-3}(?)	10^4	8×10^5	10^{-2}	10^4
Sunspots	10^7	0.2	10^{-1}	4.4×10^4	20	10^8
Solar granulation	10^6	10^{-2}	10^{-4}	8×10^3	10^3	10^7
Magnetic variable stars	10^{10}	1	10^3 (?)	8×10^5	30	3×10^{11}
Interstellar space	10^{20}	10^{-9} (?)	10^{-21} (?)	8×10^2 (?)	3×10^4	3×10^{21}
Interplanetary space	10^{11}	10^{-8}	10^{-20}	8×10^4 (?)	10^5	10^{15}
Solar corona	10^9	10^{-4} (?)	10^{-15}(?)	8×10^5 (?)	3×10^6	3×10^{15}
Dark clouds	10^{11}	10^{-10}	10^{-17}	5×10^2	30	2×10^9

$$L_u = \frac{\mu^{1/2} \sigma B l_c}{\sqrt{\rho_m}} << 1 \tag{1.6}$$

where l_c is a characteristic length of the plasma and ρ_m is the mass density. As the conductivity of known plasmas generally varies only over about four orders of magnitude, from 10^2 to 10^6 siemens/m, the value of L_u is largely dependent on the strength of B in the plasma as delineated in Table 1.6.

The variation of B in plasmas can be 18 orders of magnitude, from microgauss strengths in intergalactic space to perhaps teragauss levels in the magnetospheres of neutron sources. On earth, magnetic field strengths can be found from about 0.5 gauss (0.5×10^{-4} T) to 10^7 gauss (10^3 T) in pulsed-power experiments; the outer planets have magnetic fields reaching many gauss, while the magnetic fields of stars are 30–40 kG (3–4 T). Large scale magnetic fields have also been discovered in distant cosmic objects. The center of the Galaxy has milligauss magnetic field strengths stretching 60 pc in length. Similar strengths are inferred from polarization measurements of radiation recorded for double radio galaxies. No rotating object in the universe, that is devoid of a magnetic field, is known.

In cosmic problems involving planetary, interplanetary, interstellar, galactic, and extragalactic phenomena, L_u is usually of the order 10^{15}–10^{20} (Figure 1.16). In planetary ionospheres L_u falls below unity in the E layer. Neglecting lightning, planetary atmospheres and hydrospheres are the only domains in the universe where a nonhydromagnetic treatment of fluid dynamic problems is justified.

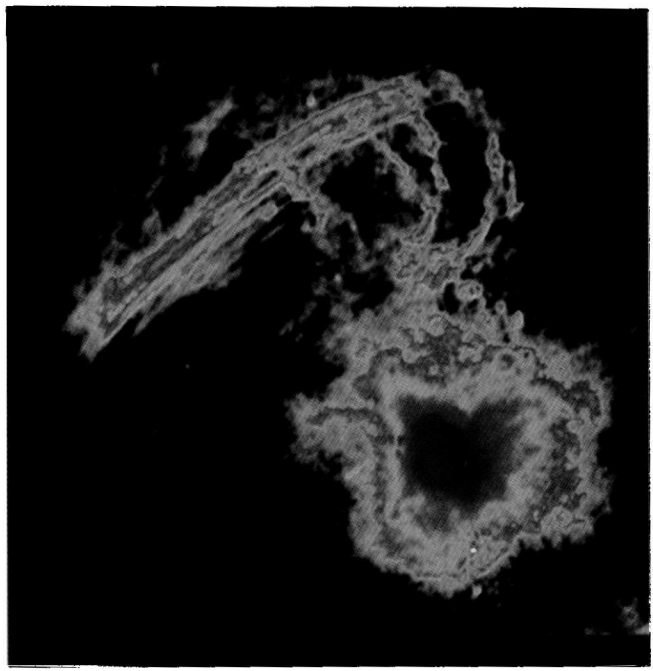

Figure 1.14. VLA radiograph of large-scale, 20-cm radio emission features within ~60 pc (20 arc min) of the Galactic nucleus. The galactic plane runs from top-left to bottom-right, through the lower diffuse structure. The contrast is chosen to bring out radio features brighter than 15 mJy per beam area (the half-power beam width is 5 × 9 arc s) (Courtesy F. Yusef-Zadeh).

1.4 Power Generation and Transmission

On earth, power is generated by nuclear and nonnuclear fuels, hydro and solar energy, and to a much lesser extent, by geothermal sources and magnetohydrodynamic generators. Always, the location of the supply is not the location of major power usage or dissipation. *Transmission lines* are used to convey the power generated to the load region. As an example, abundant hydroelectric resources in the Pacific Northwest of the United States produce power (~1,500 MW) that is then transmitted to Los Angeles, 1,330 km away, via 800 kV high-efficiency dc transmission lines. In optical and infrared emission, only the load region, Los Angeles, is visible from the light and heat it dissipates in power usage. The transmission line is *invisible* (Figure 1.17)

This situation is also true in space. With the coming of the space age and the subsequent discovery of magnetospheric-ionospheric electrical circuits, Kirchoff's circuit laws (Appendix A) were suddenly catapulted to dimensions eight orders of magnitude larger than that previously investigated in the laboratory and nearly four orders of magnitude greater than that associated with the longest power distribution systems on earth.

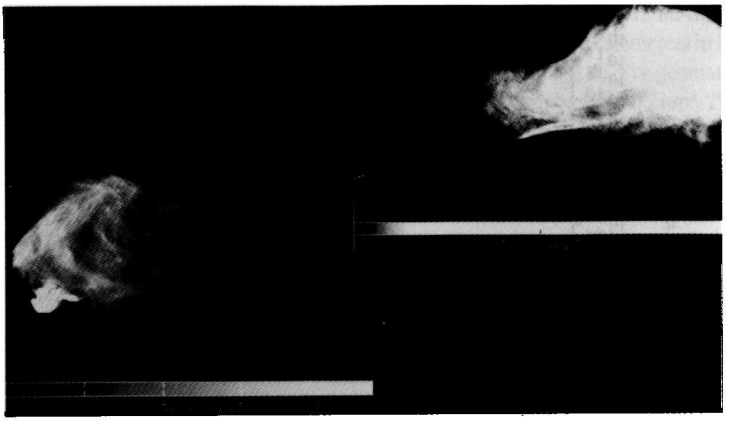

Figure 1.15. Photographic representation of Cygnus A at 6 cm wavelength with 0."4 resolution. The east-west extent of the radio emission is 127". The bars beneath each radio lobe denote the receiver sensitivity: The left-hand lobe is at about 5 mJy/pixel, while the right-hand lobe is 1.5 mJy/pixel. The plasma associated with this radio galaxy is thought to have $n \approx 2\text{–}3\times10^{-3}$ cm^{-3} and $B \approx 1\text{–}2\times10^{-4}$ G.

On earth, transmission lines consist of metallic conductors or waveguides in which energy is made to flow via the motion of free electrons (currents) in the metal or in displacement currents in a time varying electric field. Often strong currents within the line allow the transmission of power many orders of magnitude stronger than that possible with weak currents. This is because a current associated with the flow of electrons produces a self-magnetic field that helps to confine or pinch the particle flow. *Magnetic-insulation* is commonly used in pulsed-power technology to transmit large amounts of power from the generator to the load without suffering a breakdown due to leakage currents caused by high electric potentials.

There is a tendency for charged particles to follow magnetic lines of force and this forms the basis of transmission lines in space (Appendix A). In the magnetosphere-ionosphere, a transmission line 7–8 earth radii in length (R_e = 6,350 km) can convey tens of terawatts of power, that derives from the solar wind–magnetosphere coupling[7], to the lower atmosphere. The transmission line is the earth's dipole magnetic field lines along which electrons and ions are constrained to flow. The driving potential is solar-wind induced plasma moving across the magnetic field lines at large radii. The result is an electrical circuit in which electric currents cause the formation of auroras at high latitude in the upper atmosphere on earth. This aurora mechanism is observed on Jupiter, Io, Saturn, Uranus, and is thought to have been detected on Neptune and perhaps, Venus.

Only the aurora discharge is visible at optical wavelengths to an observer. The source and transmission line are invisible (Figure 1.18). Before the coming of space probes, in situ measurement was impossible and exotic explanations were often given of auroras. This is probably true of other non in situ cosmic plasmas today. The existence of a megaampere flux tube of current, connecting the Jovian satellite Io to its mother planet (Figure 1.9), was verified with the passage of the Voyager spacecraft.

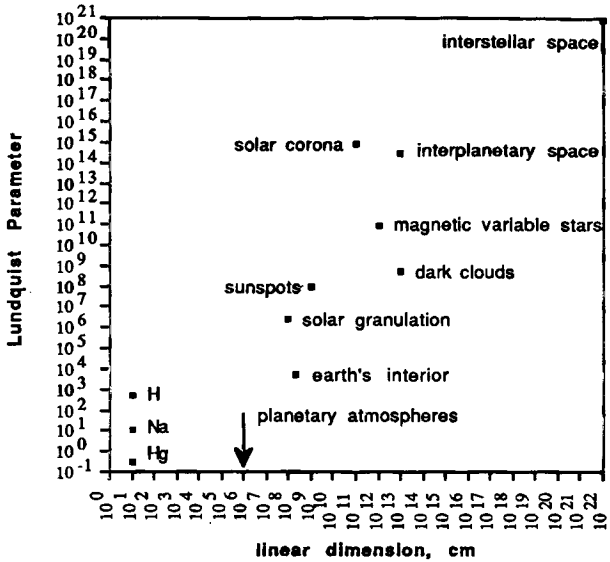

Figure 1.16. The Lundquist parameter L_u vs linear dimension for a variety of laboratory, space, and astronomical plasmas.

1.5 Electrical Discharges in Cosmic Plasma

An electrical discharge is a sudden release of electric or magnetic stored energy. This generally occurs when the electromagnetic stress exceeds some threshold for breakdown that is usually determined by small scale properties of the energy transmission medium. As such, discharges are local phenomena and are usually accompanied by violent processes such as rapid heating, ionization, the creation of pinched and filamentary conduction channels, particle acceleration, and the generation of prodigious amounts of electromagnetic radiation.

As an example, multi-terawatt pulsed-power generators on earth rely on strong electrical discharges to produce intense particle beams, X rays, and microwaves. Megajoules of energy are electrically stored in capacitor banks, whose volume may encompass 250 m^3. This energy is then transferred to a discharge region, located many meters from the source, via a transmission line. The discharge region, or load, encompasses at most a few cubic centimeters of space, and is the site of high-variability, intense, electromagnetic radiation (Figure 1.2).

On earth, lightning is another example of the discharge mechanism at work where electrostatic energy is stored in clouds whose volume may be of the order of 3,000 km^3. This energy is released in a few cubic meters of the discharge channel.

The aurora is a discharge caused by the bombardment of atoms in the upper atmosphere by 1–20 keV electrons and 200 keV ions spiralling down the earth's magnetic field lines at high latitudes. Here, the electric field accelerating the charged particles derives from plasma moving across the earth's dipole magnetic field lines many earth radii into the magnetosphere. The

potential energy generated by the plasma motion is fed to the upper atmosphere by multi-megaampere Birkeland currents (Chapter 2) that comprise a transmission line, 50,000 kilometers in length, as they flow into and out of the discharge regions at the polar horns (Figure 1.5). The generator region may encompass 10^{12}–10^{13} km^3 while the total discharge volume can be 10^9–10^{10} km^3. The stored or generated and radiated energies and powers versus linear dimension (approximately, the cube root of the volume) of several cosmic plasma discharge objects are shown in Figure 1.19.

1.6 Particle Acceleration in Cosmic Plasma

1.6.1 Acceleration of Electric Charges

The acceleration of a charged particle q in an electromagnetic field is mathematically described by the Lorentz equation Eq.(1.5),

$$\mathbf{F} = m\mathbf{a} = q(\mathbf{E} + \mathbf{v} \times \mathbf{B}) \tag{1.7}$$

The electric field vector **E** can arise from a number of processes (Chapters 4 and 5) that include the motion of plasma with velocity **v** across magnetic fields lines **B**, charge separation, and time varying magnetic fields via Eq.(1.1).

Acceleration of charged particles in laboratory plasmas is achieved by applying a potential gradient between metallic conductors (cathodes and anodes); by producing time varying magnetic fields such as in betatrons; by radio frequency (RF) fields applied to accelerating cavities as in linear accelerators (LINACS); and by beat frequency oscillators or wake-field accelerators that use either the electric field of lasers or charged particle beams to accelerate particles.

The magnetospheric plasma is essentially collisionless. In such a plasma, electric fields aligned along the magnetic field direction (Chapter 3) freely accelerate particles. Electrons and ions are accelerated in opposite directions, giving rise to a current along the magnetic field lines (Chapter 2).

1.6.2 Collective Ion Acceleration

The possibility of producing electric fields by the space-charge effect to accelerate positive ions to high energies was first discussed by Alfvén and Wernholm (1952). They were unsuccessful in their attempt to experimentally accelerate ions in the collective field of clouds of electrons, probably because of the low intensity of electron beam devices available then. However, proof of principle came in 1961 when Plyutto reported the first successful experiment in which ions were collectively accelerated. By 1975, the collective acceleration of ions had become a wide-spread area of research. Luce (1975) reported collectively accelerating both light and heavy ions to multi-MeV energies, producing an intense burst of D–D neutrons and nuclear reactions leading to the identification of several radioisotopes. Luce used a plasma-focus device (Section 4.6.2) and attributed the collective beam to intense current vortex filaments in the pinched plasma (Section 1.7). Subsequently, Destler, Hoeberling, Kim, and Bostick (1979) collectively accelerated carbon ions to energies in excess of 170 MeV using a 6 MeV electron beam.

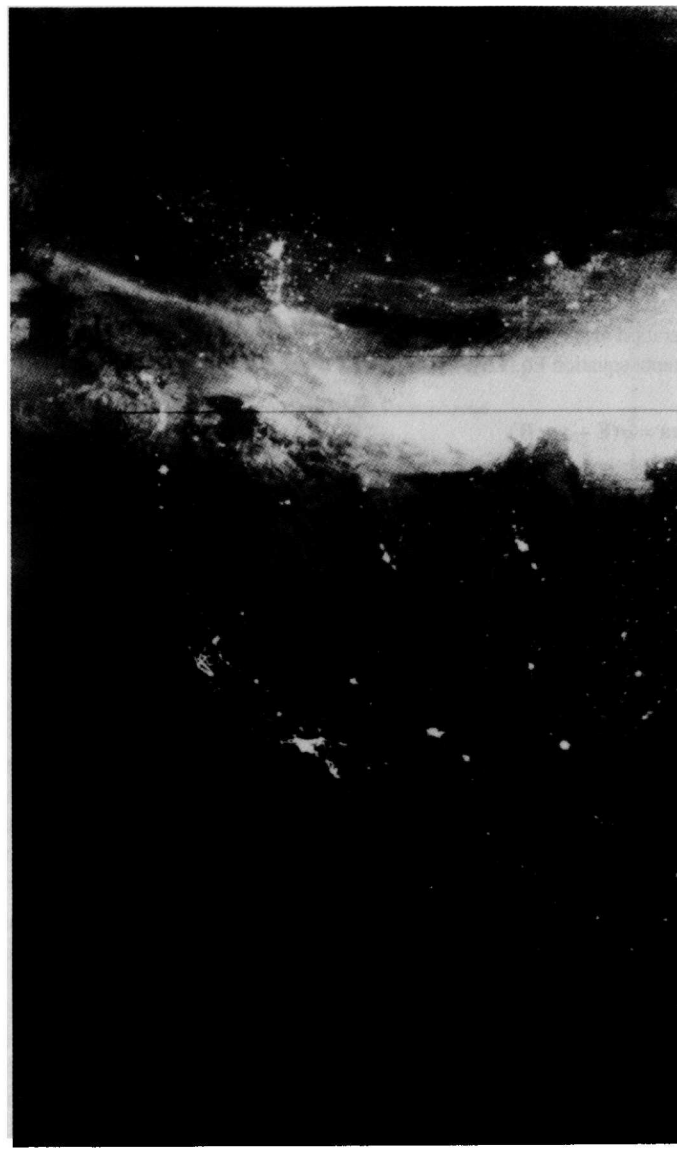

Figure 1.17. White light view of North America on the evening of 13 March 1989. Photo taken by the Department of Defense F9 meteorology satellite. Visible light radiation defines major metropolitan areas, while other land features are illuminated by moonlight. The white band at the top of the photograph is an aurora. The

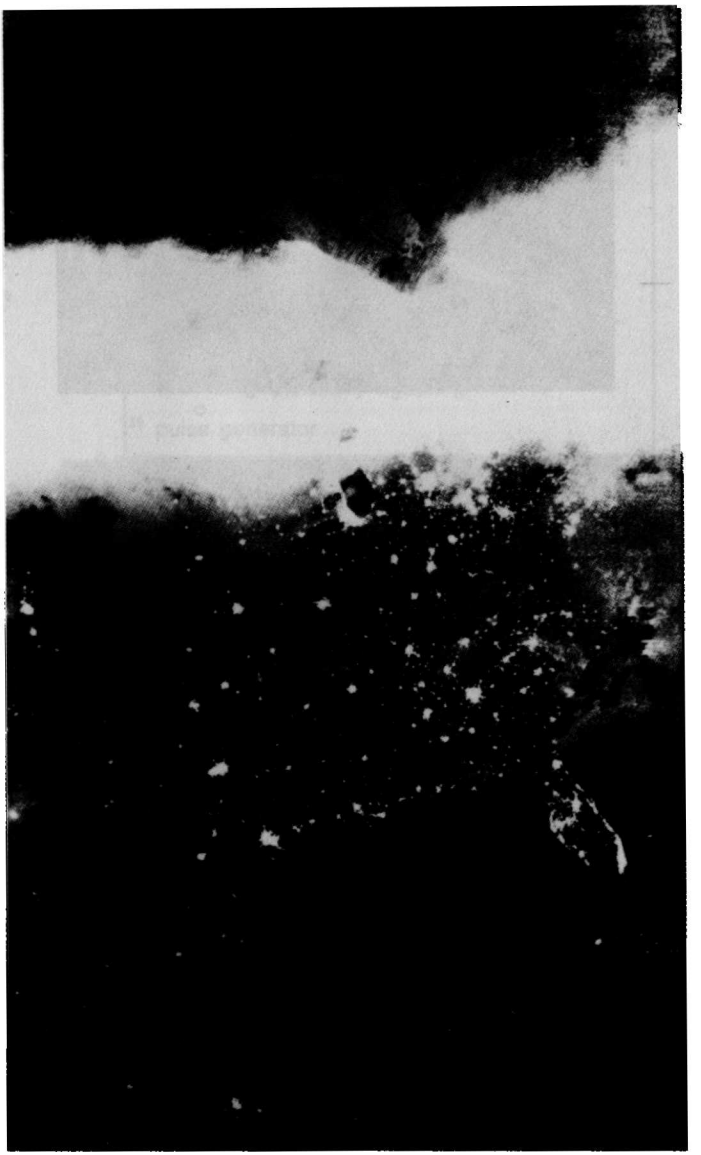

eastern half of this composite image was obtained around 4:00 Universal time on 14 March, about three hours after the auroral peak display. The western half was taken one orbit (roughly 100 min) later, during which the aurora intensity had decreased substantially (courtesy of Frederick Rich, Air Force Geophysics Laboratory).

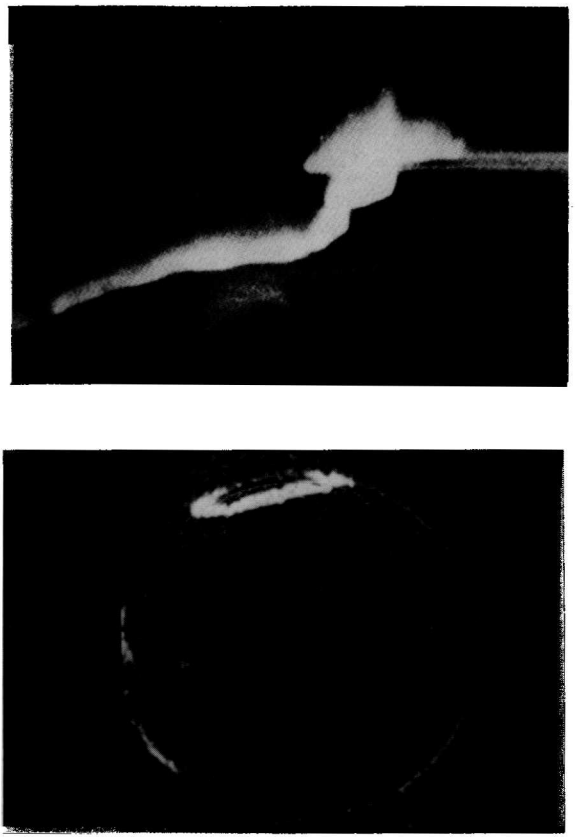

Figure 1.18. (top) The aurora photographed from the space shuttle Challenger (photo taken by Don Lind). **(bottom)** The aurora borealis photographed in ultraviolet light by the Dynamic Explorer satellite.

Individual ion energies up to several GeV using pulsed-power generators have been suggested in particle-in-cell simulations of collective ion acceleration processes [Faehl and Godfrey 1978; Shanahan and Faehl 1981].

Collective acceleration as a mechanism for creating high energy ions in astrophysical plasmas were investigated by Bostick (1986).

1.7 Plasma Pinches and Instabilities

1.7.1 The Bennett Pinch

In cosmic plasma the perhaps most important constriction mechanism is the electromagnetic attraction between parallel currents. A manifestation of this mechanism is the pinch effect as first

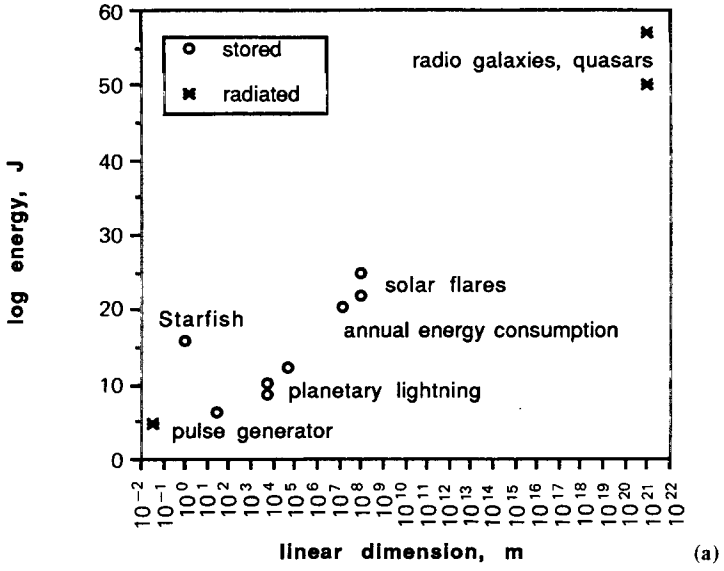

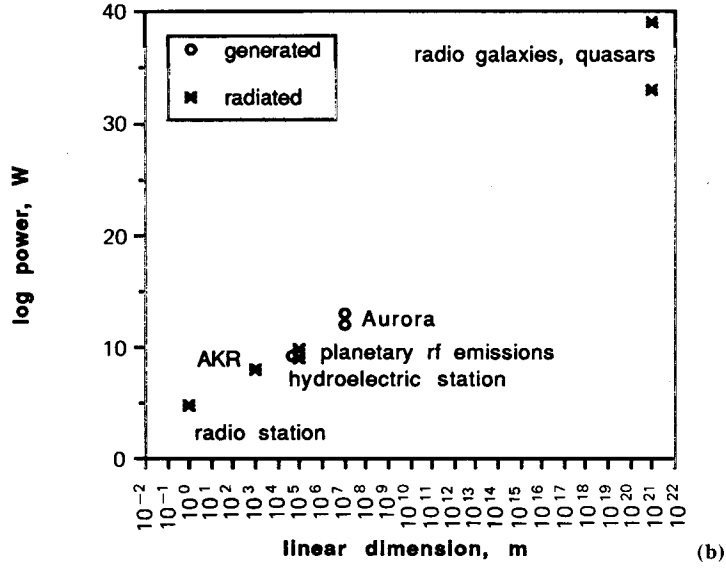

Figure 1.19. (a) Stored and radiated energies from man-made and natural plasmas versus linear dimension. Mankind's total energy consumption in 1989 is shown for comparison. (b) Generated and radiated power versus linear dimension.

studied by Bennett (1934). Phenomena of this general type also exist on a cosmic scale and lead to a bunching of currents and magnetic fields to filaments. This bunching is usually accompanied by the accumulation of matter, and it may explain the observational fact that cosmic matter exhibits an abundance of filamentary structures.

Consider a fully ionized cylindrical plasma column of radius r, in an axial electric field E_z, that produces an axial current density j_z. Associated with j_z is an azimuthal magnetic field B_ϕ. The current flowing across its own magnetic field exerts a $\mathbf{j} \times \mathbf{B}$, radially inward, pinch force. In the steady-state, the balance of forces is

$$\nabla p = \nabla(p_e + p_i) = \mathbf{j} \times \mathbf{B} \tag{1.8}$$

By employing Eq.(1.2), $\nabla \times \mathbf{B} = \mu_0 \mathbf{j}$, and the perfect gas law $p = N\,k\,T$, we arrive at the Bennett relation

$$\boxed{2N\,k(T_e + T_i) = \frac{\mu_0}{4\pi} I^2} \tag{1.9}$$

where N is the number of electrons per unit length along the beam, T_e and T_i are the electron and ion temperatures, I is the total beam current, and k is Boltzmann's constant.

1.7.2 The Force-Free Configuration

Sheared magnetic fields $(\nabla \times \mathbf{B} \neq 0)$ are a characteristic of most plasmas. Here, the sheared field is considered a nonpotential field $(\nabla \times \mathbf{B} \neq 0)$ that is caused by shear flows of plasma. A nonpotential field tends to settle into a particular configuration called a "force-free" field, namely

$$(\nabla \times \mathbf{B}) \times \mathbf{B} = 0 \tag{1.10}$$

or

$$\boxed{\mathbf{j} \times \mathbf{B} = 0} \tag{1.11}$$

since $\mathbf{j} = \nabla \times \mathbf{B}\ \mu_0^{-1}$, showing that the electric current tends to flow along $\mathbf{B}$. Substituting (1.11) into (1.8) gives $\mathbf{F} = \nabla p = 0$, hence the name "force-free". Force-free fields tend to have a twisted or "sheared" appearance. Examples of force-free fields are chromospheric fibrils and penumbral structures near active sunspots (Sects. 3.7.2 and 5.6.2).

The condition (1.10) can be satisfied in three ways: $\mathbf{B} = 0$ (trivial), $\nabla \times \mathbf{B} = 0$ (i.e., $\mathbf{j}$=0), or

$$\nabla \times \mathbf{B} = \alpha\,\mathbf{B} \tag{1.12}$$

where the scalar $\alpha=\alpha(r)$ in general. The essence of a force-free field is simply that electric currents flow parallel to magnetic field lines. Such currents are often called "field-aligned" currents (Chapter 2).

The force-free fields with constant α represent the lowest state of magnetic energy that a closed system may attain. This has two important consequences. It proves the stability of force-free fields with constant α, and shows that in a system in which the magnetic forces are dominant and in which there is a mechanism to dissipate the fluid motion, force-free fields with constant α are the natural end configuration. In astrophysical plasmas, the dissipation mechanism may be the acceleration of charged particles to cosmic ray energies.

1.7.3 The Diocotron Instability

One of the outstanding problems in the propagation of electron beams along an axial magnetic field is the breakup of the beam into discrete vortex-like current bundles when a threshold determined by either the beam current or distance of propagation is surpassed. The phenomena observed, closely resembles that associated with the Kelvin–Helmholtz fluid dynamical shear instability, in which vortices develop throughout a fluid when a critical velocity in the flow is exceeded, with a large increase in the resistance to flow [Chandrasekhar 1961].

While structural changes in the azimuthal direction are observed in solid, annular, or sheet beams, it is with thin electron beams that the vortex phenomenon is most pronounced. Since thin annular beams are easily produced and are capable of conducting intense currents, they have found widespread application in microwave generation and accelerators. Conversely, in many applications a cold beam is desired and the heating of the beam by the onset of instabilities is an undesired property.

The instability leading to the filamentation of the beam is known as the "slipping steam" or "diocotron"[8] and occurs when charge neutrality is not locally maintained, for example, when electrons and ions separate. In the steady state Eq.(1.3) in cylindrical coordinates is

$$r^{-1}\frac{d(rE_r)}{dr} = -\frac{e}{\varepsilon_0}(n_e - n_i) \tag{1.13}$$

which gives rise to a shear in the drift velocity. The shear (precisely, the axial component of the vorticity) is given by

$$\omega_s = (\nabla \times \mathbf{v})_z = \frac{1}{r}\frac{\partial (rE_r/B_z)}{\partial r}$$

$$= \frac{e}{\varepsilon_0 B_z}(n_e - n_i) = q\,\omega_\gamma(1 - f_e) \tag{1.14}$$

where

$$q = \frac{\omega_p^2}{\omega_\gamma^2} \tag{1.15}$$

is called the cross-field electron beam parameter [Buneman et al. 1966], $\omega_p^2 = n_e e^2 / m_e \gamma \varepsilon_0$, and $\omega_\gamma = \omega_b / \gamma = -e B / m_e \gamma$, where γ is the Lorentz factor $\gamma = (1 - \beta_z^2)^{-1/2}$, and $\beta_z = v_z / c$ for a beam of axial velocity v_z. The factor $f_e = Z n_i / n_e$ represents the degree of charge neutralization. For strong magnetic field "low-density" beams ($q < 0.1$) of thickness Δr, the instability occurs at long wavelengths

$$\lambda \approx (\pi / 0.4)\, \Delta r \tag{1.16}$$

or at wavelengths about eight times the beam thickness.

Equations (1.13)-(1.15) are exactly the magnetron equations (c.f. "Buneman Small Amplitude Theory" in Collins, *Microwave Magnetrons*), except that $n_i = 0$ in a properly vacuum-pumped magnetron.

Figure 1.20 depicts both the vortices of a 90 kA electron beam etched onto a carbon witness plate and those of a 58 μA electron beam detected by a sensitive fluorescent screen. Therefore, in the laboratory, well-defined vortices are found to occur over some 12 orders of magnitude in beam current. This mechanism was first introduced to explain auroral curtains (Figure 1.21) by Alfvén (1950). The diocotron instability as the cause of the auroral curtains is discussed in Section 2.9.8.

1.7.4 Critical Ionization Velocity

If both a plasma and a neutral gas are so thin that collisional momentum exchange is negligible, one would expect them to move through each other without appreciable interaction. That this need not be so was suggested by Alfvén (1942) in his theory of the origin of the planets and satellites. He introduced the hypothesis that if the relative velocity exceeds a certain critical value, a strong interaction and rapid ionization of the neutral gas would take place. He further assumed that this "critical velocity" v_c was given by the velocity at which the neutral gas particles with mass M have a kinetic energy equal to their ionization energy eV_i:

$$\frac{1}{2} M v_c^2 = e V_i \tag{1.17}$$

Table 1.7 summarizes the critical ionization velocity parameters for many elements while Figure 1.22 illustrates the gravitational potential energy versus ionization potential [Alfvén and Arrhenius 1976].

At the time Eq.(1.17) was proposed, there was no known reason why such a relation should hold. Nevertheless, the hypothesis was confirmed later in a laboratory experiment [Fahleson 1961]. For many years it remained a mystery, but experiments have now clarified the phenomenon at least in general terms. What is involved is an instability that transfers energy from ions to electrons, so that they become capable of ionizing. Still, important questions remain [Brenning and Axnäs 1988].

Meanwhile, critical ionization velocity phenomena have been observed in space plasma [Haerendel 1982, Torbert 1988]. The phenomenon has been invoked in several cosmical appli-

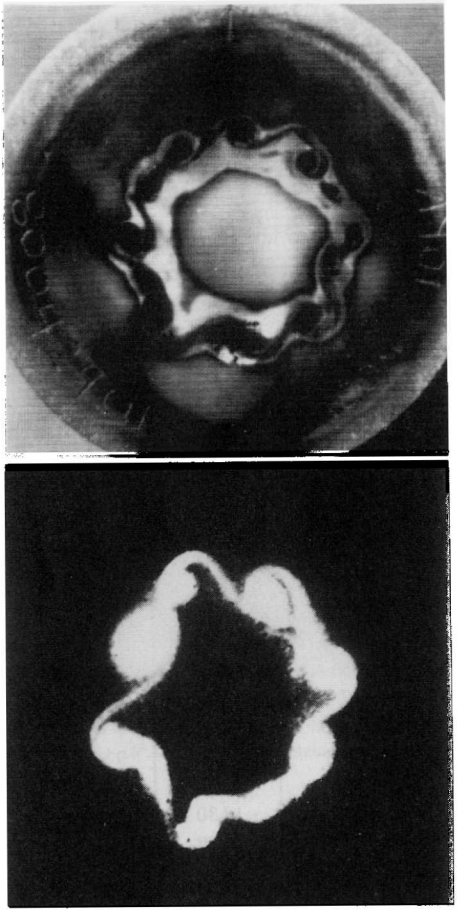

Figure 1.20. **(top)** Vortices of a 90-kA electron beam etched onto a carbon witness plate (courtesy of H. Davis). **(bottom)** Vortices of a 58-μA electron beam photographed on a fluorescent screen (courtesy of H. F. Webster).

cations, such as the formation of an ionosphere at the Jovian satellite Io [Cloutier 1978], the interaction of the solar wind with gas clouds [Lindeman et al. 1974, Gold and Soter 1976], with comets [Haerendel 1986, Galeev et al. 1986], with planetary atmospheres [Luhmann 1988], and with the interstellar medium [Petelski et al. 1980, Petelski 1981]. Thus, the phenomenon may have important astrophysical implications. However, these cannot be evaluated in detail until a full understanding of the phenomenon has been achieved, which is the goal of rocket experiments.

Table 1.7. Parameters associated with the critical ionization velocity

Element[a]	Ionization potential volts	Average atomic mass amu	Gravitational potential energy (log) g/cm	Atomic abundance [b] Si = 10^6	Critical velocity (10^5 cm/sec) (km/sec) (mm/μsec)	Band
H	13.5	1.0	20.29	2×10^{10}	50.9	I
He	24.5	4.0	19.94	2×10^{9}	34.3	I
Ne	21.5	20.2	19.18	2×10^{6}	14.3	II
N	14.5	14.0	19.18	2×10^{6}	14.1	II
C	11.2	12.0	19.11	1×10^{7}	13.4	II
O	13.5	16.0	19.08	2×10^{7}	12.7	II
(F)	17.42	19.0	19.11	4×10^{3}	13.3	II
(B)	8.3	10.8	19.08	1×10^{2}	12.1	II
[Be]	9.32	9.0	19.18	8×10^{-1}	14.1	II
[Li]	5.39	6.9	19.04	5×10^{1}	12.2	II
Ar	15.8	40.0	18.78	1×10^{5}	8.7	III
P	10.5	31.0	18.70	1×10^{4}	8.1	III
S	10.3	32.1	18.70	5×10^{5}	7.8	III
Mg	7.6	24.3	18.60	1×10^{6}	7.7	III
Si	8.1	28.1	18.60	1×10^{6}	7.4	III
Na	5.12	23.0	18.30	6×10^{4}	6.5	III
Al	5.97	27.0	18.48	8×10^{4}	6.5	III
Ca	6.09	40.1	18.30	7×10^{4}	5.4	III
Fe	7.8	55.8	18.30	9×10^{5}	5.2	III
Mn	7.4	54.9	18.30	1×10^{4}	5.1	III
Cr	6.8	52.1	18.30	1×10^{4}	5.0	III
Ni	7.6	58.7	18.30	5×10^{4}	5.0	III
(Cl)	13.0	35.5	18.70	2×10^{3}	8.4	III
(K)	4.3	39.1	18.30	2×10^{3}	4.6	III

[a] Minor elements (abundance 10^2-10^4) are indicated by parentheses; trace elements (abundance < 10^2) are indicated by brackets.

[b] The very fact that separation processes are active in interstellar and circumstellar space makes it difficult to specify relative abundances of elements except by order of magnitude and for specific environments (such as the solar photosphere, the solar wind at a given point in time, the lunar crust). The abundances are the averages estimated by Urey (1972). Most values are based on carbonaceous chondrites of Type II which form a particularly well analyzed set, apparently unaffected by the type of differentiation which is characteristic of planetary interiors. Supplementary data for volatile elements are based on estimates for the solar photosphere and trapped solar wind. All data are normalized to silicon, arbitrarily set at 10^6.

Because the existence of this anomalous interaction has been so definitely documented plus the fact that it has been so successfully applied to the cosmogonic process, should make it interesting to keep in mind in cosmological contexts, too.

Figure 1.21. Auroral vortices observed in the magnetic zenith, College, Alaska, 31 January 1973. The exposure time is 0.1 s and the field of view is 12 × 16°. The image was obtained from a low-light level television system with a broad-band red-light filter (courtesy T. Hallinan).

1.8 Diagnosing Cosmic Plasmas

1.8.1 The Electromagnetic Spectrum

For millennia our knowledge of the universe has been based on information received in the visual octave, 400–800 nm, supplemented during the last half-century by infrared and radio observations (Figure 1.23). During the 1970s and 1980s, however, space research has opened the full spectrum, including the entire infrared region and the ultraviolet, X ray, and γ ray regions (Figure 1.24). The full electromagnetic spectrum is delineated into *bands*, which generally are designated as follows:

Gamma Ray and X ray. Most emission at these wavelengths is likely to be produced by electrons with energies in excess of 10^2 eV. We know that processes in magnetized plasmas, especially concerning electric fields aligned by magnetic fields, accelerate auroral electrons to keV energies. Similar plasma processes in solar flares produce energies of 1–10 GeV. Under cosmic conditions, relativistic double layers (Chapter 5) may generate even higher energies in magnetized cosmic plasmas.

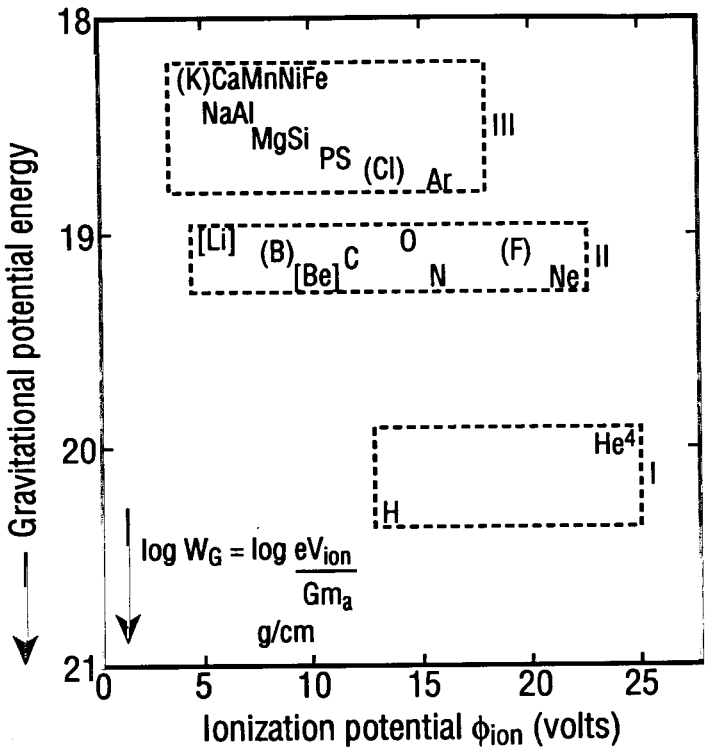

Figure 1.22. The gravitational energy W_G and ionization potential of the most abundant elements. Roman numerals refer to row in the periodic table, with "III" including the fourth role. All elements in a band have approximately the same gravitational energy and ionization potential as discussed by Alfvén and Arrhenius (1976).

Therefore we can assume with some confidence that the X rays and γrays we observe derive mainly from magnetized plasmas with energies in excess of 10^2 eV. Therefore, we call the picture we get from these wavelengths the high-energy-plasma universe, or simply, the *plasma universe*.

High energy magnetized plasmas not only emit X rays and γrays, but also synchrotron radiation that often falls in lower energy bands, including the optical and radio regions.

The energy densities of radiation in the γ ray and X ray bands are ~10^{-18} J m^{-3} and ~10^{-16} J m^{-3}, respectively, and may arise from the total contribution of discrete sources (Section 6.7.5). The isotropy of the X ray background is $\Delta T/T < 10^{-2}$

Figure 1.23. (Opposite) Cross section through the earth's atmosphere showing the altitude and the approximate wavelength coverage of the different spacecraft, rockets, balloons, and ground-based observatories that make the observations. The solid white line shows the altitude as a function of wavelength where the intensity of the solar radiation is reduced to half its original value (from Max 91/courtesy of R. Canfield and B. Dennis/NASA-GSFC).

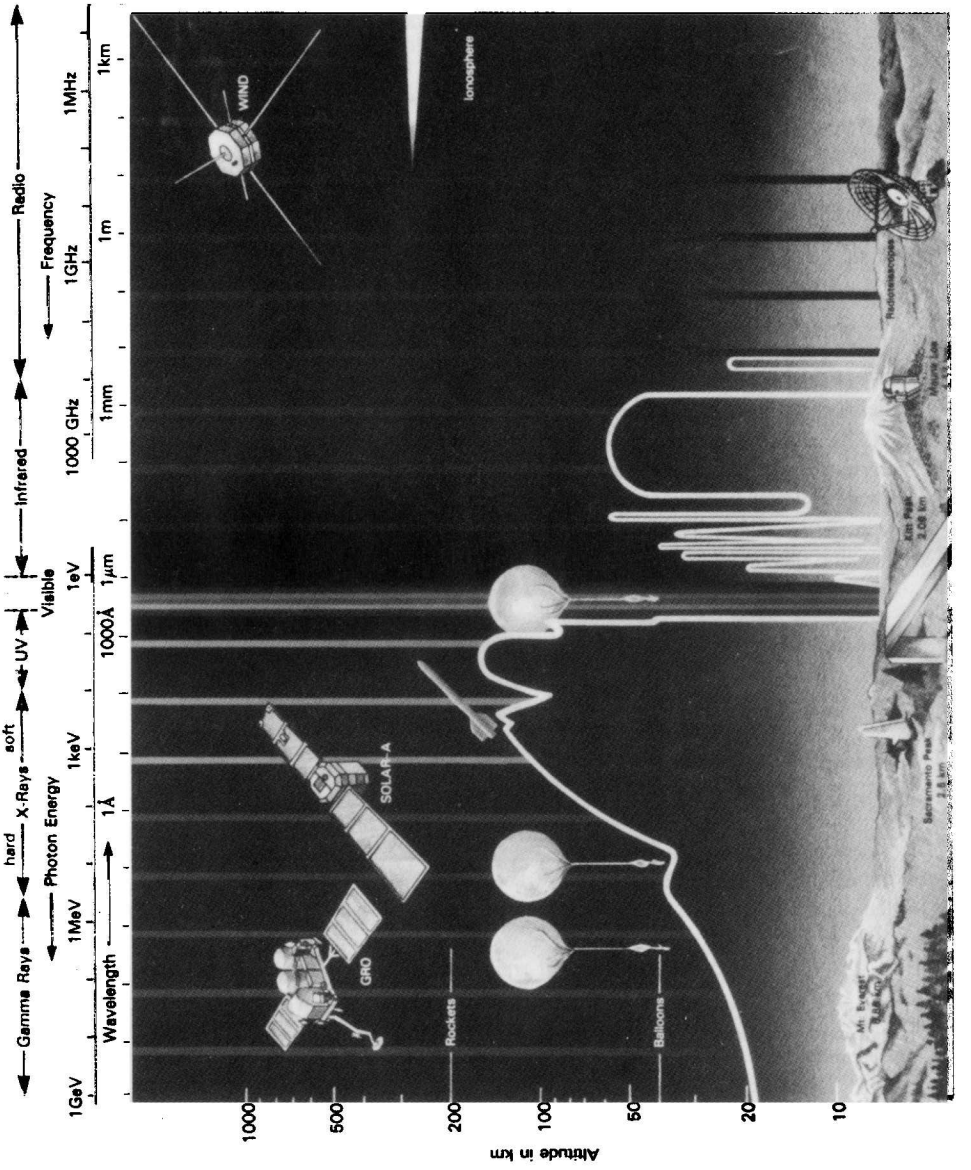
Gamma Rays
hard
X-Rays
soft
UV
Visible
Infrared
Radio
Photon Energy
Frequency
1GeV
1MeV
1keV
1eV
1000 GHz
1GHz
1MHz
Wavelength
1Å
1000Å
1μm
1mm
1m
1km
GRO
SOLAR-A
WIND
Rockets
Balloons
Ionosphere
Altitude in km
1000
500
200
100
50
20
10

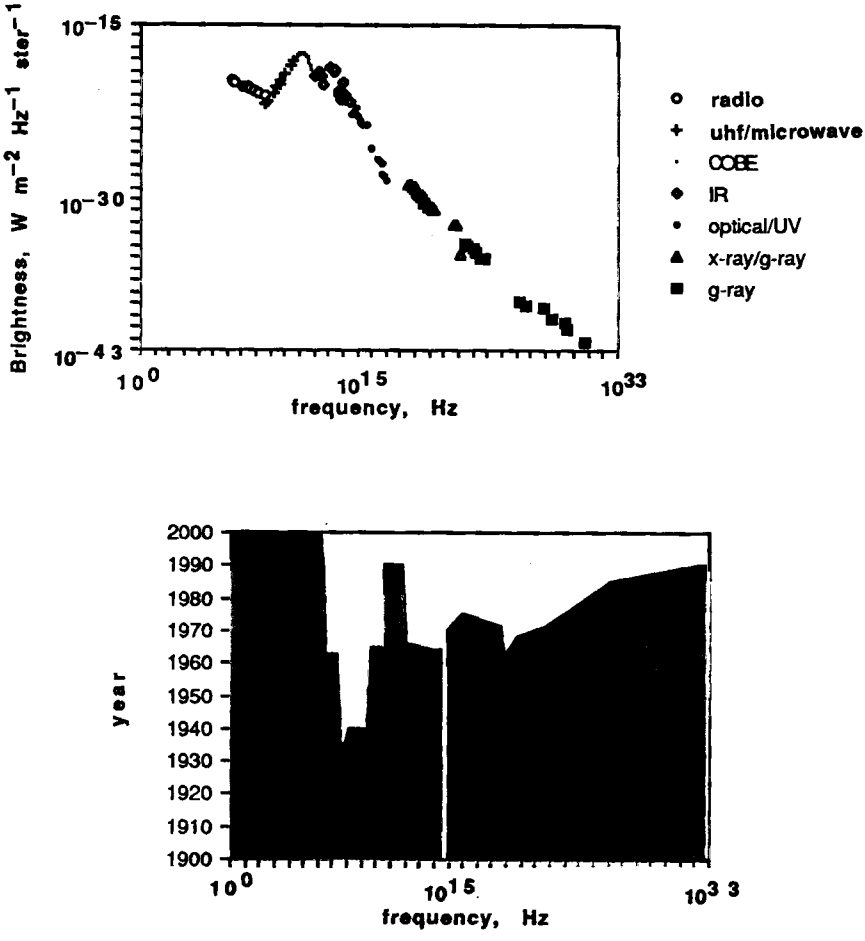

Figure 1.24. **(top)** Spectrum of the cosmic background radiation from 10^6 Hz to 10^{31} Hz. **(bottom)** The approximate year when new technology made possible observation in the different regions of the electromagnetic spectrum. As shown, most of the spectrum was not accessible until the mid-1970s.

Ultraviolet. Ultraviolet astronomy satellites have discovered various circumstellar plasma distributions in association with a variety of stellar objects, from protostars to highly evolved red giants. The energy density of the cosmic diffuse ultraviolet background is estimated to be $\sim 10^{-15}$ J m^{-3}.

Visible. Visible light comes from solid bodies such as planets, but to a much larger extent comes from stellar photospheres, which are typically plasmas with low energies – less than 10 eV. Hence

the *visual universe* is almost synonymous with the low-energy plasma universe. The energy density of visible light in the universe is $\sim 10^{-15}$ J m^{-3}.

Infrared. Infrared radiation is emitted from the photospheres of stars. For example, 52% of the electromagnetic radiation emitted by the Sun falls between 100 and 1 mm. The energy density of radiation in the infrared approaches 10^{-14} J m^{-3}. The infrared background radiation is a component of the cosmic background radiation that also includes the submillimeter and microwave backgrounds.

Submillimeter and Microwave. High-power microwave generation on earth belongs exclusively to devices using relativistic electron beams. The microwaves derive from naturally occurring beam instabilities or from electromagnetic-induced beam instabilities caused by cavities or slow-wave structures placed near the beam. For example, the diocotron instability (Section 1.7.3) is responsible for microwave generation in magnetrons and magnetically-insulated-transmission-line oscillators. Microwaves from beam interactions with slow-wave structures or cavities is the mechanism used by backward-wave oscillators and relativistic-klystron oscillators (Section 2.7.2). In addition high-power microwaves are generated via the Barkhausen-Kurz, or reflex, mechanism whenever the current carried by the relativistic electrons exceeds the space charge limiting current (Section 2.5.3) causing the formation of virtual cathodes or virtual anodes (double layers) [Peratt 1985]. A relativistic electron beam that does not produce microwave radiation is unknown.

These same basic mechanisms are likely to have their natural analogs in cosmic plasmas. Coronal loops conducting electric currents on the Sun produce microwaves, as do electric currents in the lobes of double radio galaxies. The nuclei of spiral galaxies radiate at microwave frequencies and are even sites of MASER (microwave amplification by stimulated emission of radiation) action [Moran 1984]. In our Galaxy water-vapor masers occur in the dusty plasma surrounding newly formed massive stars.

Measurements in the frequency range 400 MHz to 600 GHz show a cosmic microwave background (CMB) that can be fitted to a black body spectrum (Section 7.3) at temperature of 2.73 K (Figure 1.25).

In the Rayleigh–Jeans region (< 120 GHz) the radiation is isotropic with a precision approaching (and in some cases better than) $\Delta T / T < 3 \times 10^{-5}$ in a scale of 1° at $\lambda = 7.6$ cm [Berlin et al. 1983]. The isotropy is $\Delta T / T < 10^{-4}$ over all angular scales[9] (Figure 1.26) [Pariiskii and Korolkov 1986].

The energy density of microwaves in the universe is $\sim 4.5 \times 10^{-14}$ J m^{-3}.

Radio Wave. The radio wave portion of the electromagnetic spectrum is further divided into subclassifications.

Like Jupiter and Saturn, the earth is an intense source of long (kilometer) wavelength radio waves. These waves were discovered by satellites above the ionosphere. Since their frequency $\omega << \omega_p$, where ω_p is the maximum angular plasma frequency in the ionosphere, they cannot penetrate the ionosphere and so cannot be detected at ground level. The radiation derives from the polar aurora at high altitudes (auroral kilometric radiation or AKR). The mean intensity of AKR from earth is 100 MW, with peak intensities as high a gigawatt.

Both Jupiter and Saturn radiate at kilometric, hectometric, and decametric wavelengths via the synchrotron process (Chapter 6). The average power radiated by Jupiter between 500 and 40

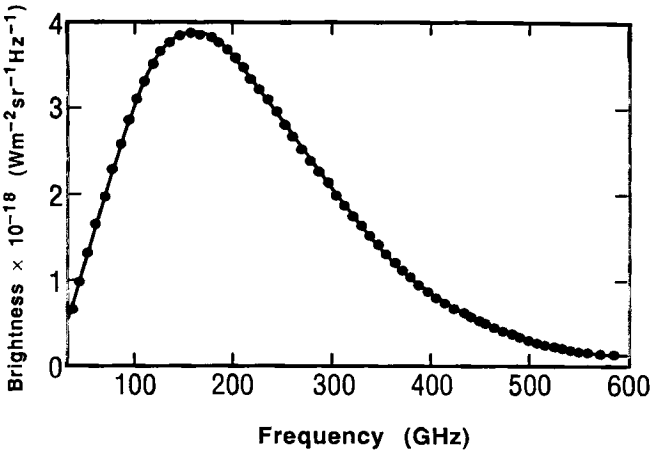

Figure 1.25. Spectral brightness vs frequency for the cosmic microwave background measured by COBE at the north galactic pole. The solid curve is a 2.735 ± 0.06 K blackbody spectrum.

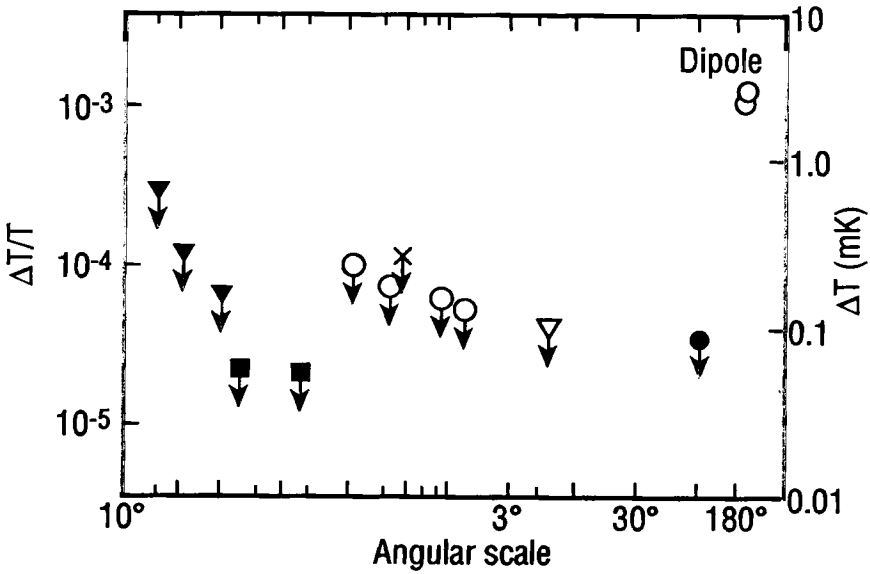

Figure 1.26. Isotropy observations in the cosmic microwave background on all angular scales. Except for the dipole effect at 180° all results are upper levels. Symbols indicate the sources of the data: (closed triangles) Very Large Array interferometer, Socorro, New Mexico; (closed squares) 140' telescope, Green Bank, West Virginia; (open circles) RATAN-600 telescope in Zelenchukskaya, USSR; (crosses) Testa Grigia alpine station, Italy; (open triangles) balloon launched from Sicily; (closed circles) balloons launched from Palestine, Texas, and São José dos Campos, Brazil.

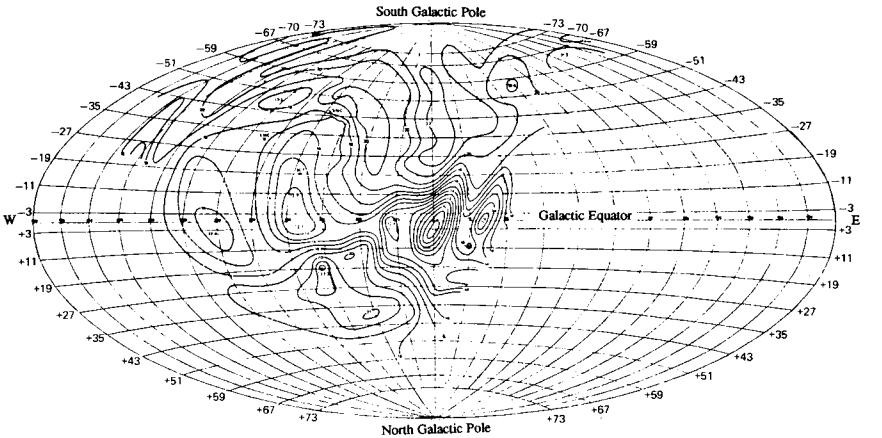

Figure 1.27. Map of southern sky at 144 meters wavelength (2.085 MHz). This map shows a bright background (corresponding to 3.5×10^6 K black body) with dimming at the center of the Galaxy and along the Milky Way (courtesy of G. Reber).

kHz is 6 GW while Saturn produces an average power of 1 GW between 3 kHz and 1.2 MHz. The planetary radio emissions are superimposed onto a cosmic radio background.

At VHF frequencies (178 MHz), the radio background radiation has a nonthermal, isotropic component whose brightness temperature (Section 7.3) is 65±5 K [Bridle 1967]. Reber (1986) has surveyed the southern sky at 2.085 MHz (144 m) and reports a bright background corresponding to a 3.5×10^6 K blackbody (Figure 1.27).

Because of the uncertainties in radio intensity at ultra-low frequencies, the energy density of radio waves in the universe is unknown but, nevertheless, appreciable.

1.8.2 In Situ Space Probes

Until the early 1970s, almost everything we knew about the universe had been obtained from information brought to the observer by electromagnetic radiation. Only a very small part of our knowledge stemmed from material information carriers, be they in the form of meteorites hitting the surface of the earth, cosmic ray particles, or material collected by manned or unmanned satellites or from lunar and planetary landings.

With the advent of earth and interplanetary space probes, this knowledge has been augmented by in situ measurements in our own solar system. These measurements have often resulted in discoveries that were unsuspected or misinterpreted from information contained in the electromagnetic spectrum alone. For example, prior to space probe measurements, it was universally

assumed that the outer magnetosphere was populated by hydrogen plasma from the solar wind, and therefore ultimately from the sun. In contrast to this, we now know that the magnetosphere is sometimes dominated by oxygen plasma originating in the earth's own atmosphere. Electric fields within the near-earth plasma were generally not thought possible until space probes measured them directly. Their existence was either not inferable by means of electromagnetic radiation or they have radiation signatures at frequencies far below that currently measurable on earth.

It is a sobering fact that even after hundreds of satellites had circled the earth, the generally accepted picture of our space environment was fundamentally wrong in aspects as basic as the origin and chemical composition of matter in the earth's own neighborhood and the existence and role of electric fields in the magnetosphere. This must inspire caution in making assertions about the composition and properties of other invisible cosmic objects, whether they be stellar interiors, interstellar plasma, pulsar magnetospheres, or intergalactic cosmic rays. The danger of misconception is particularly great for distant astrophysical objects that will forever remain inaccessible to in situ observation. To avoid this danger, it is essential to utilize the empirical knowledge of plasma behavior that has been, and will continue to be, gathered from plasmas in the laboratory and accessible regions of space.

Notes

[1] Oliver Heaviside was the first to reduce Maxwell's 20 equations in 20 variables to the two equations (1.1) and (1.2) in vector field notation. For some years Eqs. (1.1)–(1.4) were known as the *Hertz–Heaviside Equations*, and later A. Einstein called them the *Maxwell–Hertz Equations*. Today, only Maxwell's name is mentioned [Nahin 1988].

[2] These are "rewritten" in update form ideal for programming. This also emphasizes the causality correctly: $\nabla \times \mathbf{E}$ is the cause of changes in $\mathbf{B}$, $\nabla \times \mathbf{H}$ is the cause of changes in $\mathbf{D}$.

[3] In free space $\varepsilon = \varepsilon_0 = 8.8542 \times 10^{-12}$ farad m^{-1} and $\mu = \mu_0 = 4\pi \times 10^{-7}$ henry m^{-1}.

[4] One of the Sun's outstanding problems is the temperature of the corona. The temperature rises steadily in the chromosphere, then jumps abruptly in the corona to a level 300 times hotter than the surface. That the Sun is a plasma and not just a hot gaseous object is illustrated by the fact that the temperature increases away from its surface, rather than cooling as dictated by the thermodynamic principle for matter in the nonplasma state.

[5] For decades the preferred explanation has been that energy flows from the Sun's surface to the corona in the form of sound waves generated by convective upswelling motions. However, space-based ultraviolet observations proved that sound waves do not carry energy as high as the corona. One mechanism that may produce coronal heating is electron beams produced in double layers in coronal loops (Chapter 5). These are expected to accelerate electrons to energies comparable to those in the corona. Generally, the term acceleration refers to the preferential gain of energy by a population of electrons and ions, while heating is defined as the bulk energization of the ambient plasma. Paraphrasing Kirchoff that "heating is a special kind of acceleration," one may argue, since heating and acceleration are always present in flares and in laboratory relativistic electron beams, that electron beam instabilities (Section 1.7.3) may be the source of coronal heating.

[6] The degree of ionization is defined as $n_p / (n_0 + n_p)$ where n_p is the plasma density and n_0 is the density of neutral particles.

[7] It is not known how the energy carried by the solar wind is transformed into the energy of the aurora. It has been demonstrated that the southward-directed interplanetary magnetic field is an essential ingredient in causing auroral substorms so that energy transformation appears to occur through interactions between the interplanetary and geomagnetic fields [Akasofu 1981].

[8] The term *diocotron* derives from the Greek $\delta\iota\omega\kappa\varepsilon\iota\nu$, meaning "pursue."

[9] A dipole anisotropy in the cosmic microwave background, because of the net motion of the solar system through the CMB, is measured at the 10^{-3} level [Brecker 1984].